

RESEARCH REPORT
Contract no. 93/5.10.2011
IDEI Program

Project:

**The geomagnetic field under the heliospheric forcing. Inferring Earth's
internal structure and geophysical hazard induced by solar eruptive
phenomena**

General Report (2016)

Project Director,

Dr. Crişan Demetrescu
Corresponding Member of the Romanian Academy

October, 2016

Outline

Introduction

Chapter I. New geomagnetic and magnetotelluric measurements in Romania

- 1.1. Geomagnetic measurements
 - 1.1.1. The magnetic anomaly characterizing the Secular Variation National Network stations
 - 1.1.2. The secular variation of the geomagnetic field
- 1.2. Magnetotelluric measurements

Chapter II. The crust and mantle magnetic and electric structure at the Romanian territory and European continent scales

- 2.1. Models of the lithosphere electric properties distribution for Romania
 - 2.1.1. Application of the magnetotelluric method
 - 2.1.2. Application of the magnetic induction model
- 2.2. Model of electric properties for Europe. Application of the magnetic induction model method

Chapter III. Analysis of solar eruptive processes and of solar wind, responsible for the hazardous geomagnetic activity (geomagnetic storms and substorms) during 1964 – 2014

- 3.1. Introduction
- 3.2. Coronal mass ejections
 - 3.2.1. Analysis of CMEs responsible for risk geomagnetic activity (storms with $Dst < -150$ nT) during solar cycle 23
 - 3.2.2. Analysis of CMEs/ICMEs responsible for moderate geomagnetic activity (storms with -150 nT $< Dst < -50$ nT) from solar cycle 23
- 3.3. High speed streams in the solar wind
 - 3.3.1. HSS Catalogue. HSS dynamics for the last four solar cycles (1984 – 2008)
 - 3.3.2. HSS contribution to moderate geomagnetic activity during solar cycle 23
- 3.4. On the geoeffectiveness of solar and heliospheric processes. Correlation analysis for various pairs of variables characteristic to CMEs, HSSs and geomagnetic storms

Chapter IV. Modeling of the geomagnetically induced currents (GIC) by geomagnetic storms produced by solar eruptive phenomena

- 4.1. Data and method
- 4.2. Results at the European continent scale
- 4.3. Results for the Romanian territory

Chapter V. On the geoeffectivity of solar activity prior to space era

- 5.1. Evolution of the interplanetary electric field in the last 150 years
- 5.2. On the geoeffectivity of solar activity in the last 400 years

Chapter VI. Dissemination of results

Conclusions

Introduction

The research within the frame of this contract seeks to get a better understanding of space weather effects on electrical conductive structures of the Earth's interior, with applications in deciphering the internal structure at scales of the Romanian territory and European continent, on one hand, and in the assessment of geophysical hazard at mid latitudes, induced by space weather processes, on the other. The main objectives are:

1. Inferring the magnetic and electric structure of terrestrial lithosphere and mantle at Romanian territory and European continent scales;
2. Analyzing the solar eruptive processes responsible for the hazardous geomagnetic activity (geomagnetic storms and substorms) in the timespan 1964-2014;
3. Modeling the surface geoelectric field;
4. Assessing the geophysical hazard associated to variations of the surface geoelectric field.

The research report at the end of the project is structured in chapters, according to the project research plan, modified for the years 2015 and 2016 by additional acts agreed by UEFISCDI.

In *Chapter I*, entitled "**New geomagnetic and magnetotelluric measurements in Romania**" a synthesis is presented on geomagnetic measurements at the 26 stations of the Secular Variation National Network and at the Surlari geomagnetic observatory, as well as on magnetotelluric soundings performed in the Transylvanian Depression and in the seismogenic Vrancea area. A Table with all values determined in the six years of the project, as well as maps of the geographical distribution of the geomagnetic field, maps of the crustal geomagnetic anomaly, maps of the mean secular variation in the timespan 2010.5 – 2015.5, for the four geomagnetic elements H, Z, D, F.

In *Chapter II*, entitled "**The crust and mantle magnetic and electric structure at the Romanian territory and European continent scales**", three models are presented, one for the European continent, that uses data from the geomagnetic network of observatories and nine geomagnetic storms main phase, and two for the Romanian territory, that use geomagnetic measurements at the repeat stations of the Secular Variation National Network and, respectively, magnetotelluric measurements. The magnetic induction model, previously developed by the research team, has been used. In case of magnetotelluric data, the electric structure on the Romanian territory is presented in the form of lithospheric blocks with a vertical variation of electric properties.

In *Chapter III*, entitled "**Analysis of solar eruptive processes and of solar wind, responsible for the hazardous geomagnetic activity (geomagnetic storms and substorms) during 1964 – 2014**", the solar eruptive processes and high speed streams that eventually generate geomagnetic storms in the solar cycle 23. The effect of those processes on the size of the generated storm, characterized by the geomagnetic index Dst, has been studied by means of a correlation analysis of parameters characterizing the two kinds of processes and the geomagnetic index (velocity of the coronal mass ejection, its kinetic energy, the product between the velocity of the ejection and the associated magnetic field, respectively the speed of the solar wind stream, the product between the speed and the associated magnetic field, speed step at the arrival of the high speed stream).

In *Chapter IV*, entitled "**Modeling of the geomagnetically induced currents (GIC) by geomagnetic storms produced by solar eruptive phenomena**", results for the continental scale, in case of 16 intense geomagnetic storms ($Dst < -150$ nT) of solar cycle 23, based on recordings provided by the 29 INTERMAGNET geomagnetic observatories of the European network, are presented. For the case of the strongest geomagnetic storms in cycle 23 (November 20-21, 2003, $Dst = -422$ nT) and in cycle 24 (March 15, 2012, $Dst = -223$ nT), the results of a study on the sources of recorded geomagnetic variations (magnetospheric and ionospheric currents), as well as of a study on the induced electric field by the storm-time geomagnetic variations are presented. Also, the geographic distribution of the maximum induced geoelectric field for each of the 16 intense geomagnetic storms of the study has been inferred.

In *Chapter V*, entitled "**On the geoeffectivity of solar activity prior to space era**", first results of a study regarding the evolution, prior to space era (~1964) of the solar wind and of its coupling to the terrestrial magnetosphere in the last 150 years, as well as of the solar/geomagnetic activity in the last 400 years, are presented. Such research aims at characterizing the so-called **space climate**, that will be approached in our future studies.

In *Chapter VI*, entitled "**Dissemination of results**", the list of published papers and scientific presentations at various conferences during the present project is given. Also the web page of the project has been completed. The web address is: <http://www.geodin.ro/IDEI2011/eng/index.html>.

The Report ends with the "**Conclusions**" section.

Chapter I. New geomagnetic and magnetotelluric measurements in Romania

1.1. Geomagnetic measurements

The geomagnetic measurements have been performed in the 26 repeat stations of the so-called Secular Variation National Network and at the Surlari geomagnetic observatory (Fig. 1.1.1). The field campaigns have been organized in each year of the time interval 2012 – 2016. The horizontal component H , the total field F , the magnetic declination D , and the magnetic inclination I have been determined. Measurements were performed by means of a DI-Flux LEMI 24 theodolite, two quartz horizontal magnetometers QHM, a proton magnetometer Geometrics, and a fluxgate recording magnetometer LEMI 18.

The calculated values of the geomagnetic elements have been corrected for the diurnal variation and translated to the time of the first reading of the series of measurements indicated in the procedures, by means of continuous recordings provided by the Surlari geomagnetic observatory. Then values for the middle of the year in which measurements were taken (geomagnetic epoch 20xx.5) have been calculated. Taking into account the delay of one year of communicated annual averages by the observatory, against which the field values are referenced, we show in the present report results based on values for the time interval 2012.5 – 2015.5 (Table 1.1). In Fig. 1.1.1 we give, as an example, maps of the geographical distribution of geomagnetic elements H , Z , D , and F , based on 2016 measurements reduced to the 2015.5 geomagnetic epoch (with definitive observatory data). In 2016, 4 additional stations were considered, to geomagnetically characterize the Transylvanian Depression and the bending zone of the Eastern Carpathians not covered by stations of the repeat stations network.

Table 1.1. Values of the geomagnetic elements determined each year of the time interval 2011-2016 at stations of the Secular Variation National Network

Statie	2011.5				2012.5				2013.5				2014.5				2015.5				2016			
	H (nT)	D(°)	Z(nT)	F(nT)	H(nT)	D(°)	Z(nT)	F(nT)	H(nT)	D(°)	Z(nT)	F(nT)												
Alexandria	20823	4,72	42078	47967	23031	4,75			23043	4,87	42120	48011	23064	4,62	42195	48087	23044	5,16	42220	48099	23050	5,36	42354	48220
Babadag	21001	5,71	42995	48572	22592	5,75	42981	48557	22590	5,97	43083	48646	22606	6,13	43100	48669	22604	5,98	43204	48760	22596	6,27	43257	48803
Bistrita	20912	4,92	43795	48698	21277		43818	48711	21292	5,31	43838	48736	21303	5,20	43898	48794	21293	5,03	43978	48862	21291	5,74	43981	48864
Bretcu	21158	5,45	43342	48546	21856	5,52	43346	48544	21870	5,52	43363	48566	21890	5,55	43399	48607	21873	5,88	43473	48666	21878	6,01	43535	48723
Chisineu - Cris	21308	4,35	43322	48431	21655	4,67	43320	48431	21673	4,82	43378	48490	21685	4,77	43432	48545	21677	4,97	43432	48541	21672	5,26	43570	48663
Cluj	21295	4,98	43499	48526	21510	5,14	43525	48550	21525	5,15	43550	48579	21530	5,12	43617	48641	21510	5,25	43701	48708	21520	5,40	43759	48765
Costesti	21318	4,84	42470	48143	22679	4,90			22669	4,99	42527	48191	22713	4,95	42531	48216	22686	5,09	42611	48274	22685	5,36	42736	48384
Deva	21509	4,60	42829	48179	22086	4,82	42884	48237	22086	4,72	42920	48269	22099	4,69	42943	48296	22097	4,93	43002	48347	22102	5,20	43093	48430
Dumbravita	21567	4,49	42847	48179	22039		42854	48189	22039	4,97	42907	48236	22062	4,75	42924	48262	22058	5,09	42978	48308	22047	5,33	43083	48396
Gropeni	21652	5,67	42903	48425	22453	5,64	42915	48434	22461	5,53	42953	48471	22474	5,40	43016	48533	22478	5,91	42777	48323	22456	6,03	43477	48806
Herculane	21868	4,37	42273	47919	22565	4,41	42310	47951	22577	4,57	42330	47975	22587	4,51	42365	48010	22579	4,92	42429	48063	22584	5,94	43197	48685
Husi	21934	6,08	43876	48890	21564	6,12	43915	48923	21577	5,94	43976	48984	21579	6,12	43966	48976	21595	6,43	43994	49008	21566	5,10	42514	48140
Lipova	22066	4,17	42856	48143	21934	4,33	42897	48179	21948	4,72	42906	48193	21952	4,37	42966	48249	21949	4,75	42997	48275	21941	6,47	44174	49158
Livada	22030	5,09			20979	4,99	44133	48865	20998	5,32	44096	48840	21014	5,20	44197	48938	20998	4,63	44249	48978	20994	4,95	43112	48375
Mizil	22145	5,11	42799	48371	22544	5,26	42804	48378	22543	5,39	42825	48395	22561	5,08	42866	48441	22554	5,65	42940	48503	22547	5,60	44350	49068
Negru - Voda	22364	5,39	42286	48183	23122	5,51	42272	48182	23119	5,56	42287	48194	23125	5,64	42402	48298	23114	5,60	42450	48335	23115	5,76	43043	48591
Radauti	22457	5,35	44317	49003	20902	5,46	44278	48964	20914	5,52	44352	49036	20917	5,55	44411	49090	20908	5,56	44503	49170	20915	5,62	43269	48603
Sadova	22539	4,36	41935	47926	23201	4,49	41982	47966	23208	4,59	41984	47972	23236	4,44	42035	48030	23217	4,79	42100	48077	23222	5,96	42528	48404
Saveni	22566	5,88	44877	49472	20821	6,12	44884	49478	20831	5,94	44963	49554	20837	6,24	44963	49557	20829	6,04	45012	49598	20824	5,79	44568	49232
Stamora	22599	4,08	42386	47924	22376	4,28	42416	47956	22386	4,46	42389	47937	22399	4,23	42479	48023	22385	4,64	42548	48077	22392	4,99	42164	48126
Strehaia	22679	4,82	42142	47888	22740	4,80	42161	47903	22753	4,96	42184	47929	22768	4,56	42246	47991	22819	4,97	42248	48017	22753	6,65	45130	49702
Selimbar	22675	4,85	42974	48344	22147	4,88	42988	48358	22166	5,53	43024	48398	22169	4,96	43088	48457	22153	5,15	43132	48488	22164	4,95	42635	48157
Somcuta	22745	4,83	43933	48758	21160	4,88	43953	48781	21176	5,01	43925	48763	21188	5,03	44029	48862	21194	5,49	44047	48881	21179	5,27	42396	48116
Tonea	23028	5,35	42344	48167	22962	5,32	42378	48199		5,24		48207	22974	5,42	42495	48308	22985	5,58	42501	48318	22969	5,65	43258	48605
Vaida	23202	4,69	43657	48580	21307	4,60	43693	48612	21317	4,52	43727	48646	21327	4,56	43776	48695	21321	4,83	43820	48732	21316	5,54	44183	48996
Varatec	23097	5,15	44022	48912	21304	5,35	44058	48938	21320	5,40	44086	48971	21333	5,66	44122	49009	21380	5,56	44154	49058	21327	5,72	42628	48423
Surlari	22652	4,83	42490	48164	22678	5,01	42559	48224	22687	5,12	42596	48261	22695	5,22	42634	48298	22688	5,34	42686	48341	22688	5,25	43983	48996

1.1.1. The magnetic anomaly characterizing the Secular Variation National Network stations

The maps of Fig. 1.1.1 indicate, by inflexions of isolines, the fact that some of the repeat stations might be affected by crustal geomagnetic anomalies. The latter can be evidenced by means of a geomagnetic reference field against measured values can be referenced, such as IGRF (International Geomagnetic Reference Field), that stands for the field originating in the Earth's core. In Fig. 1.1.2, such differences are shown for the epoch 2010.5 (the IGRF values were calculated using the code at the site <http://www.ngdc.noaa.gov/IAGA/vmod/igrf.html>)

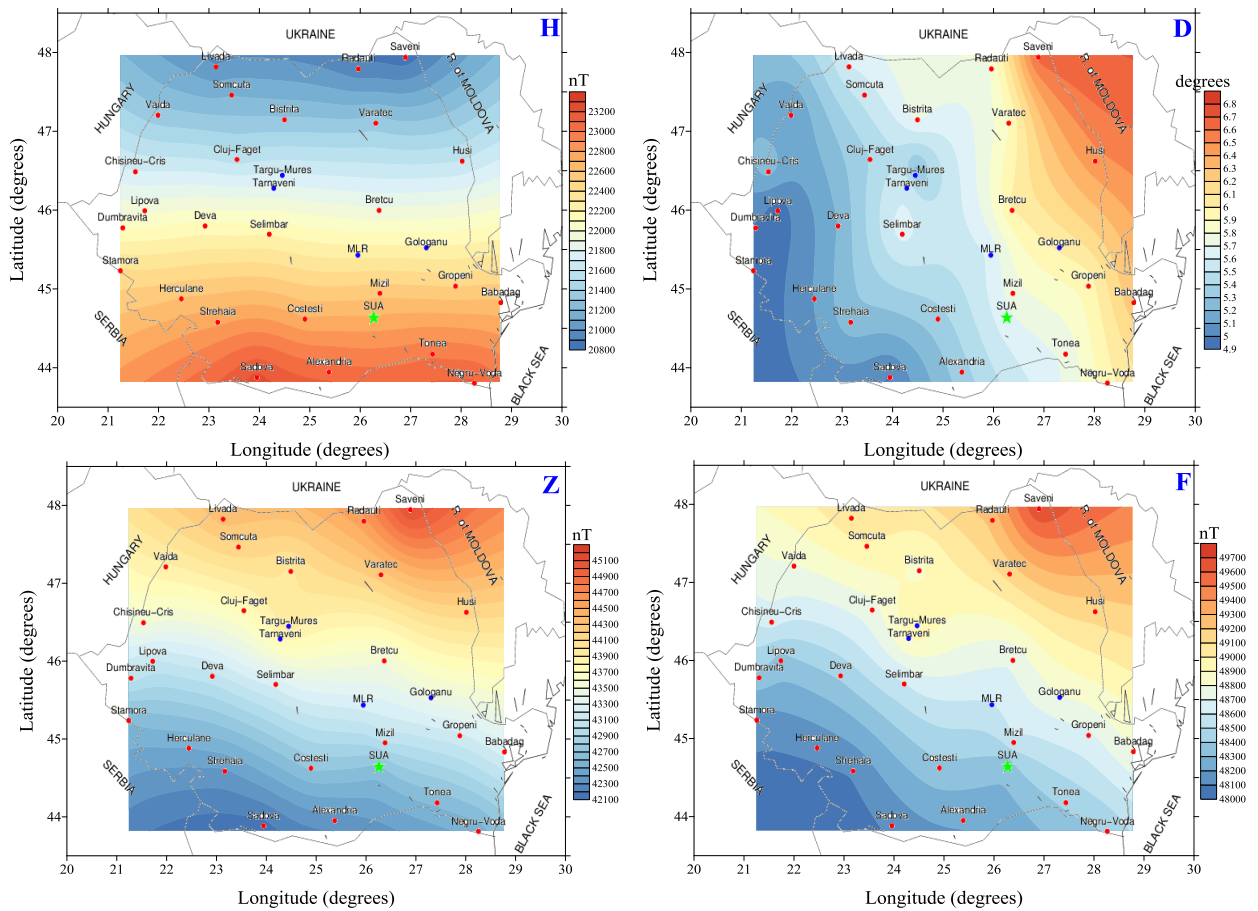


Figure 1.1.1. The geographical distribution on the Romanian territory of geomagnetic elements H, Z, D, F at epoch 2015.5 (measurements taken in 2016). The repeat stations of the network are indicated by red points, the Surlari geomagnetic observatory by green star, and the 4 additional stations by blue points

As it is known (Atanasiu et al., 1970), the repeat stations were chosen as to represent the normal geomagnetic field at that epoch. The fact that at present (after about 50 years) some of the stations show geomagnetic anomalies, reflects possible effects of the temporal variation of crustal anomalies, generally considered as constant.

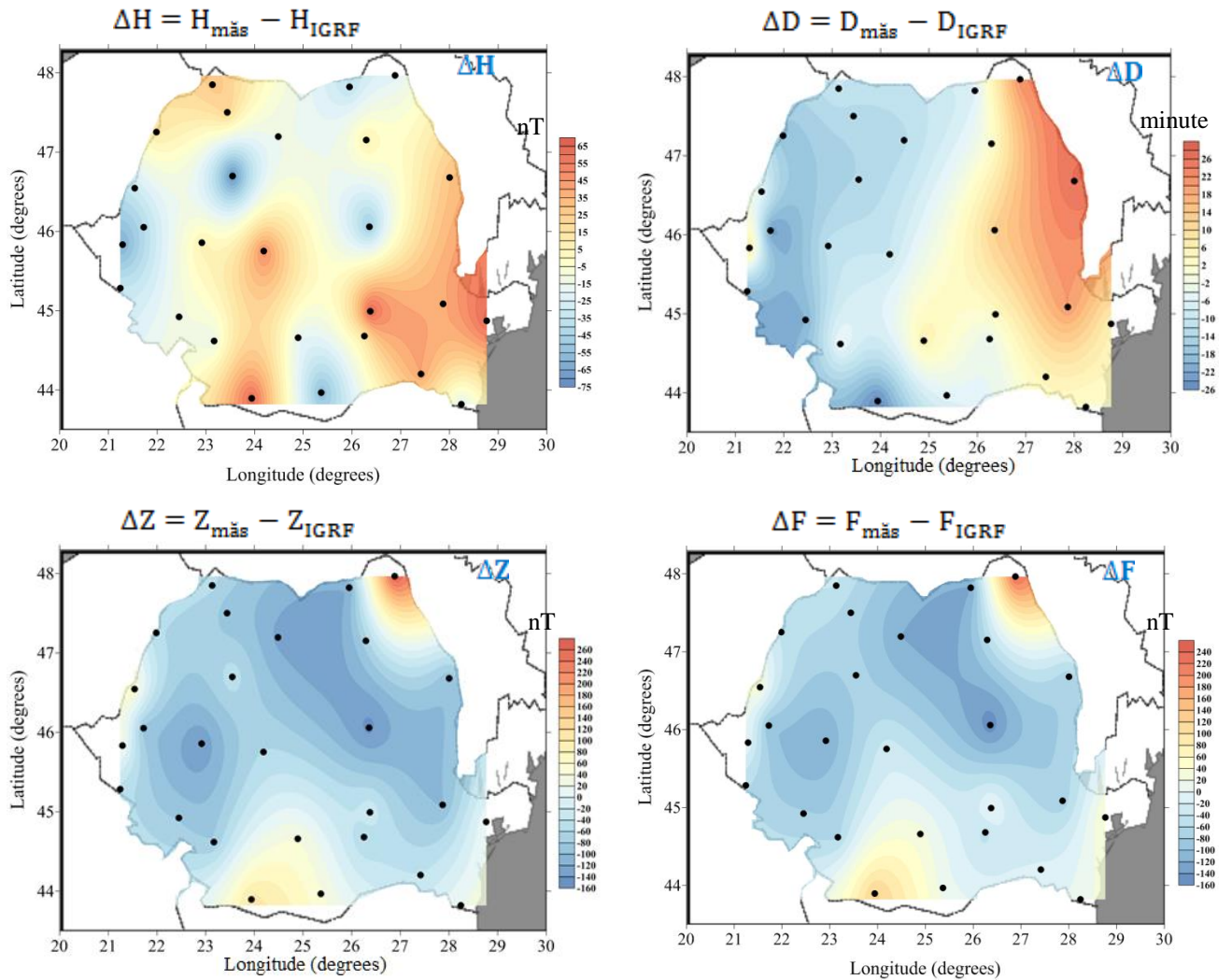


Figure 1.1.2. The geographical distribution of the crustal magnetic field at the Secular Variation Repeat Stations Network, for the geomagnetic epoch 2010.5

In the following we present the results of a study on the secular variation of the geomagnetic field on the Romanian territory in the time interval 2010 – 2014. Besides the values determined in each year of the present contract, values determined in 2010 and 2011, within the frame of a previous contracts (PN II Parteneriate 81-021/2007; PN II IDEI 151/2007) were also used.

1.1.2. The secular variation of the geomagnetic field

The evolution of geomagnetic elements in the five years of the study can be considered, in case of each station, as linear. The shape of this evolution indicates the possibility to describe the secular variation in the study interval as the slope of the straight line through the annual points. Corresponding isopore maps, from which the secular variation of the IGRF was subtracted, are given in Fig. 1.1.3. The maps show a regional distribution that is probably the consequence of lateral variation of crustal magnetic properties, as the global models of the geomagnetic field (such as IGRF) indicate a significant degree of uniformity for the secular variation on the Romanian territory.

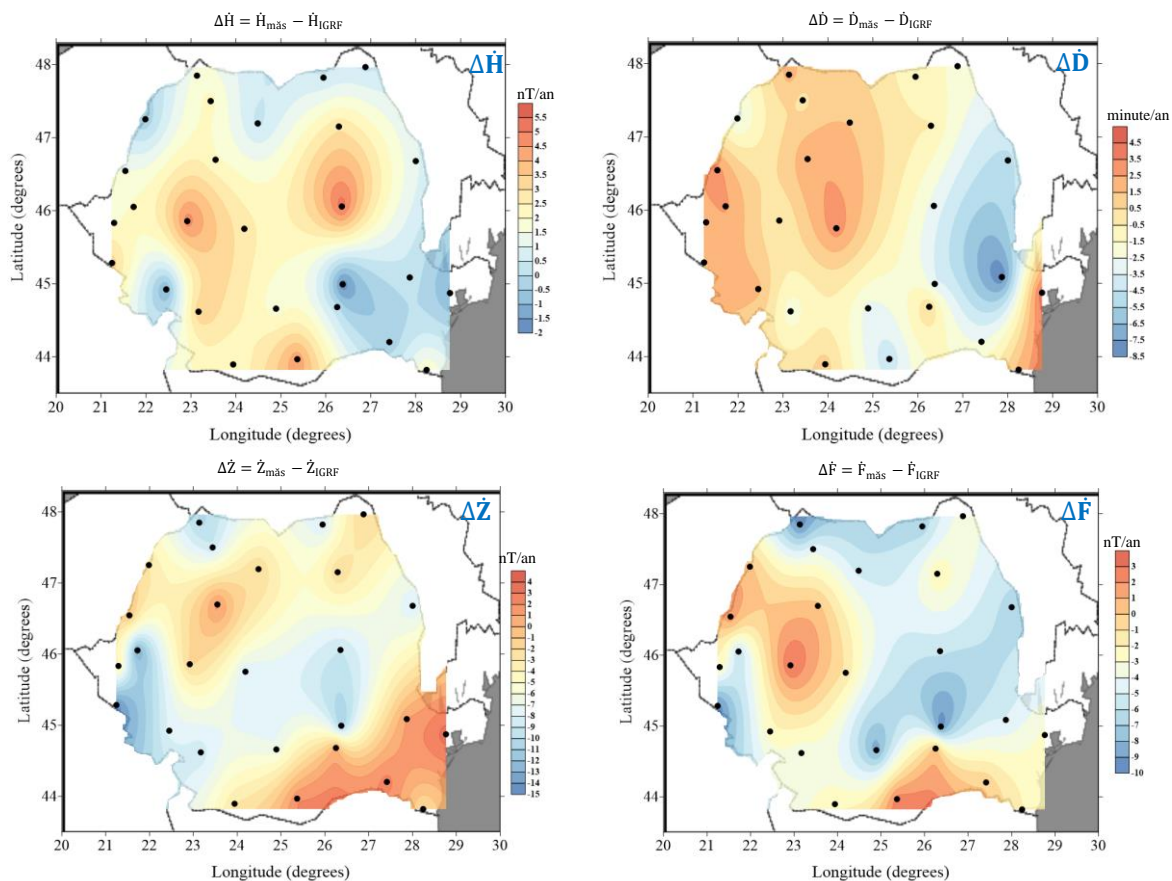


Figure 1.1.3. The geographical distribution of the mean secular variation in the time interval 2010,5–2014,5 of the geomagnetic field elements. Reference secular variation field – IGRF

Evidently, the analyzed temporal segment (2010-2014) is too short to allow approaching the debated problem in the international literature (Demetrescu and Dobrica, 2014, Thébault et al., 2009) of the time dependent magnetization of crustal rocks. Data as presented here should definitely be regarded in the context of long-term variations of the geomagnetic field, that also contain an 11-year timescale component (Demetrescu and Dobrica, 2005; 2014). Getting rid of that component in case of repeat stations requires systematic measurements during much longer timespans than in case in the present contract.

1.2. Magnetotelluric measurements

To obtain information on the vertical distribution of the electric resistivity, that would detail the magnetotelluric data in the Institute of Geodynamics archive, during the project new measurements were taken, in the Transylvanian Depression (2 stations in 2014, in the Luduș and Bazna areas) and in the Vrancea seismic area (2 stations in 2015, located close to Lopatari and Vintilă Vodă).

The multi-channel magnetotelluric equipment (GMS-06), produced by METRONIX, Germany, has been used. The central unit ADU-06 works on 5 channels to which 4 in-polarizable electric sensors for recording the electric field and 3 uni-axial, inductive-type magnetic sensors. The duration of recordings was of approximately 30 days, to get information at the crustal level and the frequency range of 10 Hz - $5 \cdot 10^{-4}$ Hz.

Recorded data are stored either in the “flashdisk” internal memory, or directly on the control computer (Laptop) HDD, on which the code MAPROS is installed. This program works under Windows 95 and controls the following operations:

1. Automatic setting of sensors (Ex, Ey, Hx, Hy, Hz) in the field;
2. Acquisition and real time data processing;
3. Robust estimation of magnetotelluric Zxy, Zyx and geomagnetic Txy, Tyx transfer functions;
4. Plotting of resistivity and phase curves (example for Lopătari, Fig. 1.2.1).

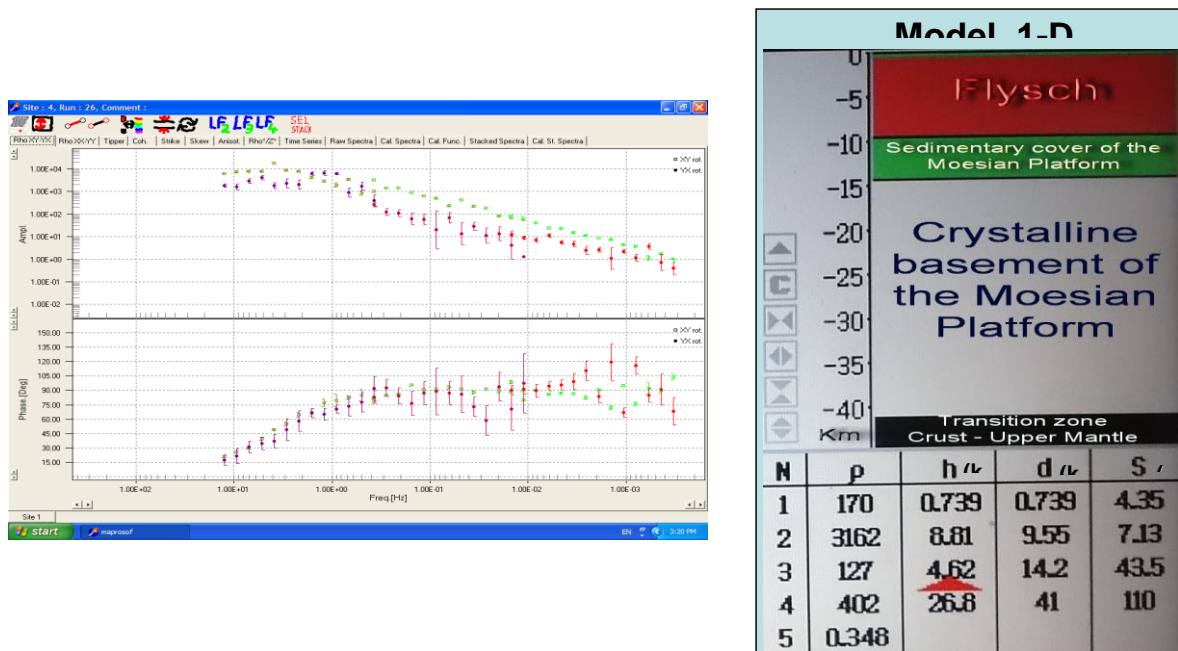


Figure 1.2.1. Left: resistivity (up) and phase (down) distributions against frequency for the magnetotelluric station Lopătari. Right: 1-D model of electrical properties

The vertical distribution of resistivity in the four measurement points has been inferred by an 1-D inversion code (IPI) and the results are presented as 1-D model in the same figure. The model was obtained after a few iterations and represents most probably the real image of the geoelectric structure in the investigated area (the foredeep of the Carpathians bend), as differences between the calculated response functions and experimental values are less than 2%. According to the given legend of the figure, the model shows the following layer thicknesses: approx. 9 km for the Carpathian Flysh nappe system; 4.6 km for the sedimentary cover of the Moesian Platform; 27 km for the crystalline basement, and resistivities of respectively 3100 Ωm , 120 Ωm , 400 Ωm . The 5th resistivity, of 0.35 Ωm is associated to the crust-mantle transition zone. In the study area the crust is approximately 40 km thick, result in accordance to other Vrance area data (Stanica et al., 2004).

References

- Atanasiu, G., Neșțianu, T., Demetrescu, C., Anghel, M., 1970, Les valeurs normales des éléments géomagnétiques, H, I, Z et F en Roumanie, pour l'époque 1967, *Rev. Roum. Géol., Géoph. Géogr., serie de Géophysique*, 14, 73-79.
- Demetrescu, C., Dobrica, V., 2005, Recent secular variation of the geomagnetic field. New insights from long series of observatory data, *Rev. Roum. Geophys.*, 49, 22-33.
- Demetrescu, C., Dobrica, V., 2014, Multi-decadal ingredients of the secular variation of the geomagnetic field. Insights from long time series of observatory data, *Phys. Earth Planet. Inter.*, <http://dx.doi.org/10.1016/j.pepi.2014.03.001>.

Stănică, D., Stănică, M., Piccardi, L., Tondi, E., Cell, G., 2004, Evidence of geodynamic torsion in the Vrancea zone (Eastern Carpathians), *Rev. Roum. de Geophysique*, 48, 15-21.

Thébault, E., Hemant, K., Hulot, G., Olsen, N., 2009, On the geographical distribution of induced-varying crustal magnetic fields, *Geophys. Res. Lett.* 36, L01307. <http://dx.doi.org/10.1029/2008GL036416>.

Chapter II. The magnetic and electric structure of crust and mantle at Romanian territory and European continent scales

2.1. Models of the lithosphere electric properties distribution for Romania

2.1.1. Application of the magnetotelluric method

Introduction

The magnetotelluric method (MT) is an electromagnetic geophysical exploration technique that images the electrical properties distribution from the Earth's subsurface to different depths. The energy of the MT is from natural sources of external origin. When this external energy, known as the primary electromagnetic field, reaches the Earth's surface, part of it is reflected back and the remaining part penetrates into the Earth. The Earth acts as a good conductor, thus electric currents (known as telluric currents) are induced which in turn produce a secondary magnetic field.

Magnetotellurics is based on the simultaneous measurement of total electromagnetic field, i.e. time variation of both magnetic field $B(t)$ and induced electric field $E(t)$. The electrical properties (e.g. electrical conductivity) of the underlying material can be determined from the relationship between the components of the measured electric (E) and magnetic field (B) variations, or transfer functions. According to the property of electromagnetic waves in the conductors, the penetration of electromagnetic waves depends on the oscillation frequency and on the conductivity of the investigated body.

The basis of the MT method was set by Tikhonov (1950) and Cagniard (1953) in the first half of the XX century. Since its inception, important developments in formulation, instrumentation and interpretation techniques have made MT as a competitive geophysical method, suitable to bring information on a broad range of geological targets.

Within the frame of the present project a synthesis and reinterpretation of MT data of the Institute of Geodynamics data archive, to which new measurements were added in areas less represented in the archive, such as the Transylvanian Depression and the Vrancea active seismic area. Basic theoretical concepts and the final model reached in this project are discussed in the next sub-sections.

Basic theoretical concepts of the magnetotelluric method

The electromagnetic field within a material in a non-accelerated reference frame can be described by the following Maxwell's equations:

$$\mathbf{J} = \sigma \mathbf{E},$$

$$\mathbf{D} = \varepsilon \mathbf{E},$$

$$\mathbf{B} = \mu \mathbf{H},$$

where σ , ε and μ describe intrinsic properties of the materials through which the electromagnetic fields propagate. σ (S/m) is the electrical conductivity [its reciprocal being the electrical resistivity $\rho = 1/\sigma$ ($\Omega.m$)]; ε (F/m) is the dielectric permittivity and μ (H/m) is the magnetic permeability; \mathbf{J} is the current density; \mathbf{D} is the displacement current in (C/m^2); \mathbf{B} is the magnetic

induction [Tesla (T) = V s m⁻²]; E (V/m) and H (A/m) are the electric and magnetic fields. These parameters are scalar quantities in isotropic media; in anisotropic materials they must be expressed tensorial. In this report, it will be assumed that the Earth properties are anisotropic.

The electrical conductivity of the Earth materials varies having a wide spectrum up to several orders of magnitude and is sensitive to small changes in minor constituents of the rock. The conductivity of a rock unit depends in general on the interconnectivity of minor constituents (fluids, partial melting) or the presence of highly conducting materials such as graphite. The conductivity of most rock materials is very low, of the order of 10⁻⁵ S/m.

Depending of the nature of the electromagnetic sources used in MT, of the properties of the Earth materials and of the depth of investigation considered, two hypotheses are applicable:

(1) Quasi-stationary approximation: Displacement currents ($\delta D/\delta t$) can be neglected relative to conductivity currents (J) for the period range 10⁻⁵s -10⁵s and for not extremely low conductivity values. Therefore, the propagation of the electromagnetic fields through the Earth can be explained as a diffusive process, which makes it possible to obtain responses that are volumetric averages of the measured Earth conductivities;

(2) Plane wave hypothesis: The primary electromagnetic field is a plane wave that propagates vertically down towards the Earth surface (z direction).

The following assumptions are also applicable in electromagnetic induction in the Earth:

- The Earth does not generate electromagnetic (EM) energy, but only dissipates or absorbs it;
- Maxwell's electromagnetic (EM) equations are obeyed;
- All electromagnetic fields are treated as conservative and analytic away from their sources.

The true resistivity of the 1-D half-space is:

$$\rho = 0.2T (|E_x|^2/|H_y|^2) \text{ or } \rho = 0.2T |Z|^2,$$

where E_x and H_y are electric and magnetic field wave vectors orthogonal to each other and the ratio E_x/H_y , named the impedance (Z), is a characteristic measure of the EM properties of the subsurface medium, and constitutes the basic MT response function.

In the case of 1-D horizontally layered structure, the true resistivity (ρ) becomes an apparent resistivity (ρ_a):

$$\rho_a = 0.2T (|E_x|^2/|H_y|^2)$$

Because of the symmetry of the problem, estimates of characteristic impedance (Z) for either a homogeneous or a layered Earth do not depend on orientation of measuring axes in the horizontal plane, so that the North and East electric field components are related to the orthogonal magnetic field components through the following linear equations:

$$E_x = Z H_y \quad \text{and} \quad E_y = -Z H_x$$

Thus, in this case at any particular period, an electric field component is linearly related to its orthogonal magnetic field component through a single valued complex scalar transfer function.

For a 2-D structure, a general MT field can be separated into two distinct modes, and these are generally referred to as E and H polarizations.

In a more complicated structure, the coupling between electric and magnetic fields is more complex. The electric fields are strongly distorted near a lateral inhomogeneity, whereas magnetic fields may be relatively less distorted.

In general, for a 3-D geoelectric structure, the impedance is expressed in matrix form in Cartesian coordinates (x, y horizontal and z positive downwards):

$$\begin{pmatrix} E_x \\ E_y \end{pmatrix} = \begin{pmatrix} Z_{xx} & Z_{xy} \\ Z_{yx} & Z_{yy} \end{pmatrix} \cdot \begin{pmatrix} H_x \\ H_y \end{pmatrix}$$

All the above relations, together with the inversion and modeling specific programs have been used to emphasize the electrical conductivity distribution at the crustal and lithospheric levels for the major structural units in Romania.

Model of electrical conductivity for the major structural units in Romania

Within the present project a synthetic model for the vertical distribution of the electrical resistivity of crust and mantle rocks on the Romanian territory, based on magnetotelluric sounding data from the Institute of Geodynamics data archive (Stănică and Stănică, 1993; Săndulescu et al., 1993; Stănică and Stănică, 1996; Stănică et al., 1996 a, b; 1997; 1999; Stănică and Stănică, 1998; Stănică et al., 2004), to which soundings performed in the 2012-2016 timespan and studies reported in various phases of the contract have been added. The resulted model describes the vertical distribution of resistivity as 1-D lithospheric models for a number of paralelipedic volumes in which the Romanian territory was divided, represented by the grid of Fig. 2.1.1. The grid, superposed on the map of magnetotelluric geotraverses on which the models are based, allow detailing and multiplication of the information that, as a matter of fact, refers to the main tectonic units on the Romanian territory, of larger dimensions. The numbers on the squares of the grid cells allow retrieving the vertical 1-D model for that lithospheric block, according to Table 2.1.1. The seven types of the resistivity vertical distribution refer to: the East European Platform + Schytian Platform + Eastern Carpathians Foredeep + North Dobrudja Orogen, model no. 1, Transylvanian Depression, model no. 2, Pannonian Depression, model no. 3, Moesian Platform + Southern Carpathians Foredeep, model no. 4, Eastern Carpathians + Neogene Volcanic Chain, model no. 5, Southern Carpathians, model no. 6, Apuseni Mountains, model no. 7. Reconsidering some magnetotelluric profiles allowed detailing information for some cells containing also crystalline structures in orogenic areas.

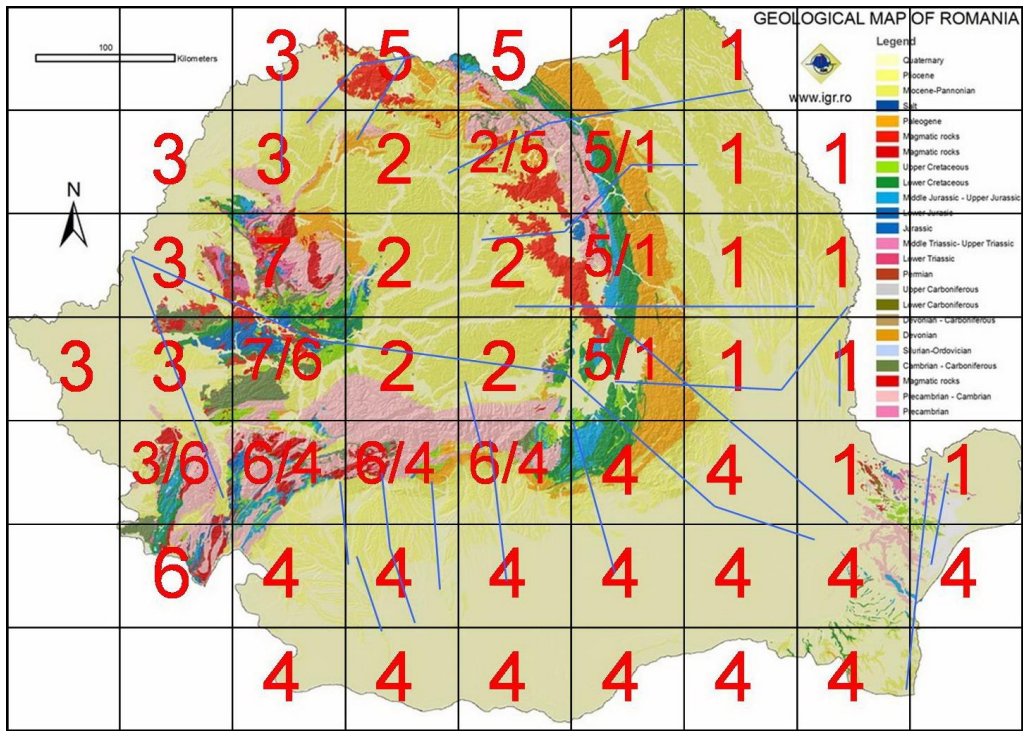


Figure. 2.1.1. The geological map of Romania, with MT geotraverses (blue) and square cells numbered from 1 to 7

Table 2.1.1. 1-D models for the vertical distribution of the electrical resistivity of the main lithosphere layers, for the seven structure types identified on the Romanian territory

Tectonic unit Model no.	Thickness (d) [km]	Resistivity (ρ) [$\Omega \text{ m} = \text{VmA}^{-1}$]
1. Est European Platform + Scythian Platform + Carpathian Foredeep + North-Dobrudjan Orogen		
Crust	10	10
	35	1000
	10	10
Litospheric Mantle	120	500
2. Transylvanian Depression		
Crust	5	5
	2	500
	20	700
	10	10
Litospheric Mantle	40	500
3. Pannonian Depression		
Crust	4	5
	16	700
	10	10
Litospheric Mantle	30	500
4. Moesian Platform		
Crust	10	10
	30	1000
	10	10
Litospheric Mantle	80	500
5. Eastern Carpathians		
Crust	3	100
	5	80
	17	10
	30	1000
	10	10
Litospheric Mantle	120	500
6. Southern Carpathians		

Crust	6	100
	7	300
	30	1000
	10	10
Litospheric Mantle	75	500
7. Apuseni Mountains		
Crust	12	330
	25	2500
	15	15
Litospheric Mantle	28	500

Based on data of Table 2.1.1, the electric properties characterizing the entire lithosphere, namely resistivity, conductivity, electrical resistance, were calculated, taking into account the thickness of the layers (Table 2.1.2). In Fig.2.1.2 maps of the calculated parameters are presented. The information of this section will be used, together with Surlari geomagnetic observatory data and the information from the repeat stations of the Secular Variation National Network to the study of induced hazards by components of the so-called space weather (e. G. geomagnetic storms).

Table 2.1.2. Electric properties of lithosphere for the seven types of structures, identified on the Romanian territory

Tectonic unit	Resistivity (ρ) [$\Omega \text{ m} = \text{V mA}^{-1}$]	Conductivity (σ) x 10^4 [$\text{S/m} = \text{AV}^{-1}\text{m}^{-1}$]	Resistance (R) [Ω]
Est European Platform + Scythian Platform + Carpathian Foredeep + North-Dobrudjan Orogen	544	18,4	95200
Transylvanian Depression	772	12,96	62525
Pannonian Depression	439	22,8	26320
Moesian Platform	540	18,5	70200
Eastern Carpathians	528	18,9	90840
Southern Carpathians	549	18,2	70300
Apuseni Mountains	1009	9,9	80685

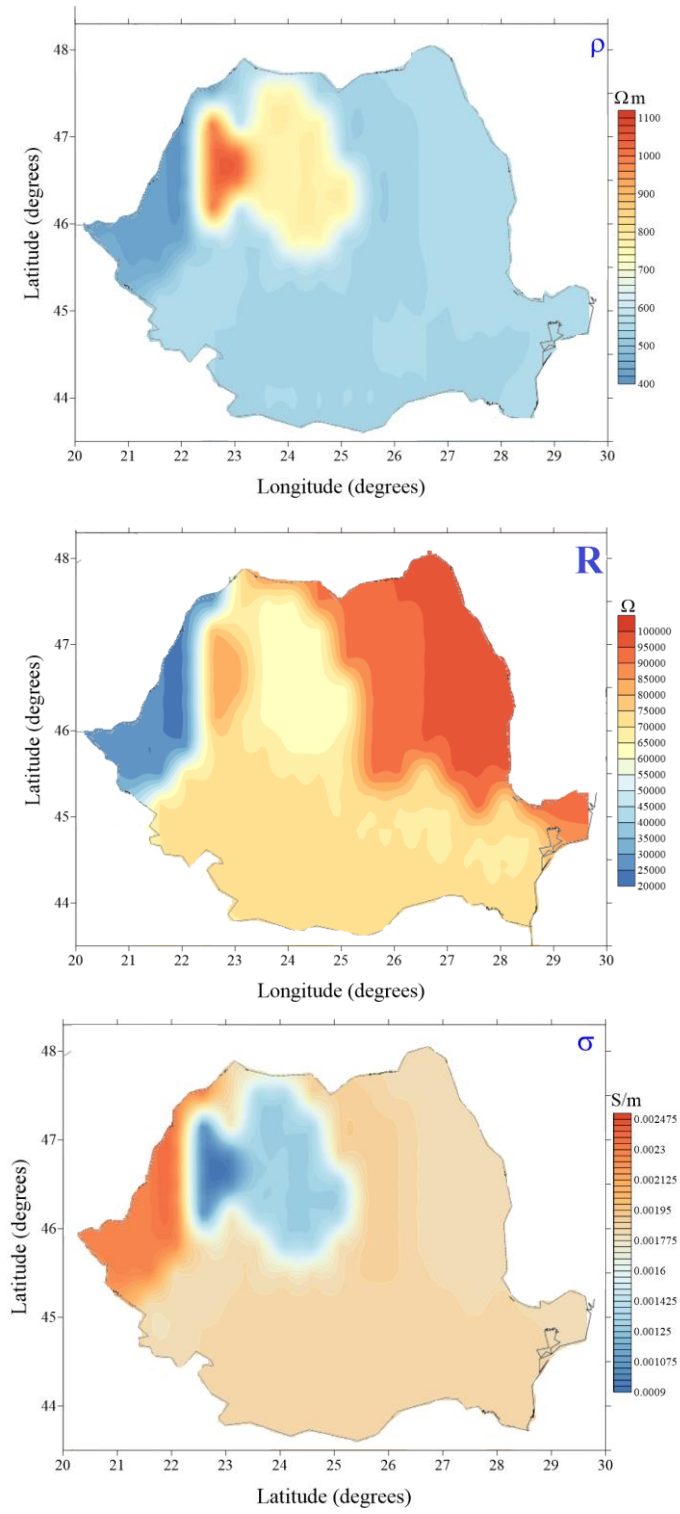


Figure 2.1.2. Electrical properties of the Romanian lithosphere, the MT method

2.1.2. Application of the magnetic induction model

The principle of the magnetic induction model method

The method we used in the present project is based on the observation that the variable external magnetic field induces variable magnetic fields not only by electromagnetic induction, but also by magnetic induction in rocks above the Curie temperature. In case of pure magnetic induction the temporal variation of the field components at a certain observation point is given by the linear combination of the inducing magnetic force (Demetrescu et al., 1985; 1988):

$$\Delta E^{(S)}(t) = \sum_{k=1}^3 C_k^E \Delta F_k(t),$$

where Δ represents variations against the temporal average, $E^{(S)}$ is the field component at the S station (E can be X, Y, Z, or F), F_k , $k = 1...3$ are the inducing force components, and C_k^E are coefficients depending of the effective magnetic permeability that characterizes the point. The calculated values of the model, $(\Delta E^{(S)}_{\text{calc}})$, represents the component of the observed signal produced by pure magnetic induction, and residuals, $(\Delta E^{(S)}_{\text{res}} = \Delta E^{(S)} - \Delta E^{(S)}_{\text{calc}})$, contain the information related to the electromagnetic induction in the Earth's interior at the considered point. The coefficients C_k^E can be determined by a least square procedure and then mapped, resulting images of the lateral (geographical) distribution of the **magnetic properties** that characterize the rock volume above the Curie temperature (generally the crust). To ensure the comparability of coefficients corresponding to various stations, recordings should be simultaneous in all stations, in order to study the same time interval proper to the inducing external force. Consequently, the mentioned temporal averages refer to the common recording interval.

Up to now, the method had been successfully applied in case of the national repeat station network (Demetrescu et al., 1985) and in case of the European network of geomagnetic observatories (Demetrescu et al., 1988; Demetrescu and Andreescu, 1992, 1994; Demetrescu and Dobrică, 2003), for the 11-year solar cycle signal, as well as in case of the Hokkaido (Japan) magnetometric network (Dobrică et al., 2008-2009), for the diurnal variation.

For the **electrical properties** of crust and mantle the residual of the magnetic induction model of the **vertical component** of the field, that responds to a much larger extent to the electromagnetic induction in crust and mantle conductive structures than the horizontal

component, was used. As the inducing electromotive force is given by the negative time derivative of the inducing magnetic field, the latter must correlate with the observed residual. In terms of a current loop in the conducting layers of the Earth's interior, the magnetic field of intensity B produced by the intensity I current flowing in the loop is given by

$$B = 2\pi k \frac{I}{a}$$

where $k = 10^{-7} \text{ WbA}^{-1}\text{m}^{-1}$ and a is the loop radius. Residuals can be viewed as a measure of the current intensity in an equivalent loop of radius unity, surrounding the observation point. This allows estimating the inductance L and resistance R of an equivalent circuit, based on the well known relationship between the instantaneous value of the tension u and the instantaneous value of the intensity i in an R-L circuit (with inductance).

$$u = L \frac{di}{dt} + Ri$$

The tension is equivalent to the negative time derivative of the inducing vertical magnetic component, and the current intensity to the residual of the magnetic induction model for the vertical component. With these equivalences, the following relationship is obtained:

$$-\dot{Z}_{sursa}(t) = L \cdot \dot{Z}_{rez}(t) + R \cdot Z_{rez}(t) \quad ,$$

where $\dot{Z}_{sursa}(t)$ is the time derivative of the vertical component of the field produced by the inducing source, and Z_{rez} is the residual of the induction model applied to the Z component recorded at the observation point. L and R can be determined by a least squares procedure for each observatory, for the given time interval. Maps with the obtained values reflect the lateral variation of electric properties of the interior. The mapped values are relative, they reflect the lateral variation, not absolute values of R and L . Also, the information that is obtained regards a large depth range, to mantle depths.

Results

As input data for the magnetic induction model for Romania, the measurements performed in 2010 in the Secular Variation National Network stations, with the additional measurements in 2016 meant to detail the network, were used. As a measure (or proxy) of external sources recordings of geomagnetic observatories Surlari (located inside the network) and Niemegek (located approximately 1000 km faraway from the network). At each station 7-8 hours long records (generally between 8 and 17 SLT (5-14 UT)) taken by magnetic variometer LEMI-18 X, Y, Z). In parallel the total field F was recorded by a Geometrics G-856 proton magnetometer. 1 minute data were used in the model.

Fig. 2.1.3 shows the distribution of crustal magnetic properties based on recordings of the vertical component Z of the geomagnetic field, for the two observatories which recording were used as proxy for the inducing force.

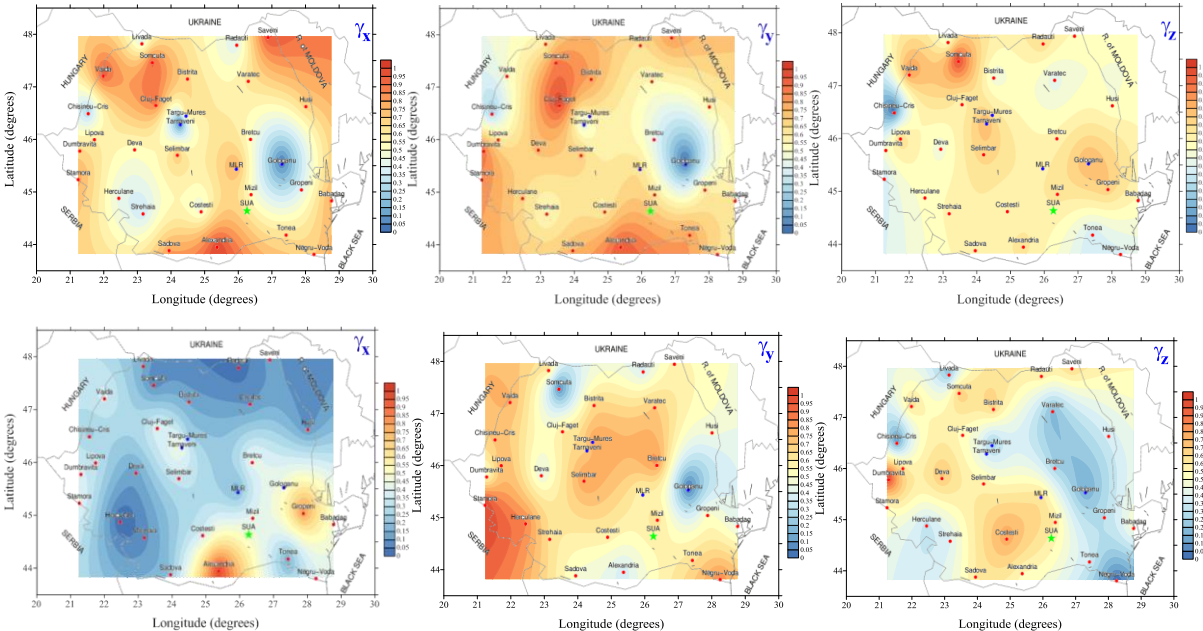


Figure 2.1.3. Magnetic properties of the crust, based on Z data. Upper plots – reference station Surlari geomagnetic observatory; lower plots – reference station Niemegek observatory

Fig. 2.1.4 shows the distribution of lithosphere electrical resistance R and induction L. To get these images, measurements taken during the 2016 campaign at the two new stations in the Transylvanian Depression and the two new stations in the Carpathian bend foredeep were also used. These stations do not usually belong to the Secular Variation National Network as being located on regional anomalies of the Transylvanian Depression size. They were included to allow a more detailed characterisation of the geomagnetic storms hazard (see Chapter IV of the report).

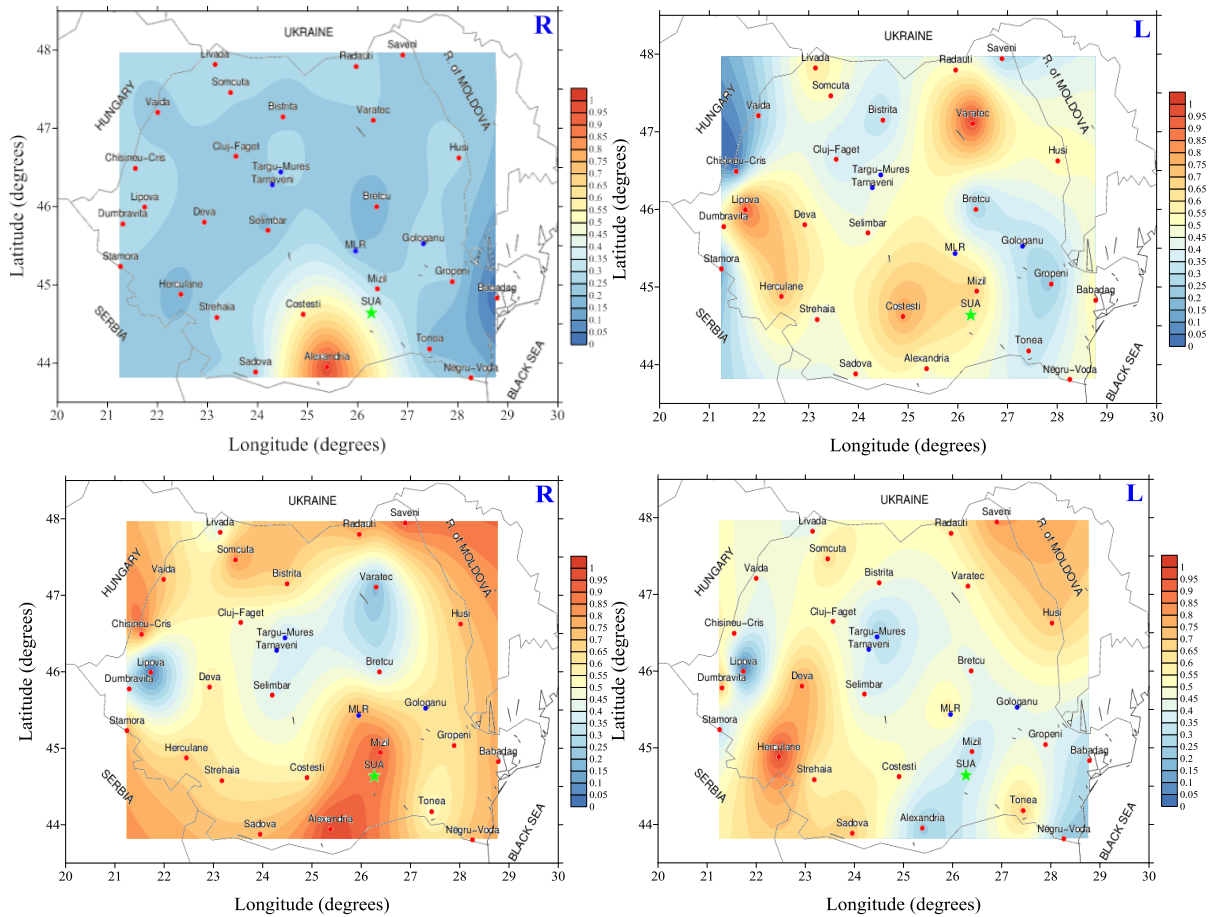


Figure 2.1.4. Geographical distribution of the electrical resistance R and inductance L on the Romanian territory. The magnetic induction method. Reference stations: Surlari observatory (upper plots), Niemeğk observatory (lower plots)

A look at the maps indicates differences between a southern area, associated to the Moesian Platform and Alexandria Depression, and the rest of the territory. The latter is characterized by small values, with a pronounced minimum in the Eastern Carpathians and SE and SW extensions (toward Dobrudja and, respectively, the Southern Carpathians bend, probably also influenced by the high conductivity Carpathian anomaly path (Stănică et al., 2000; Report stage 2015). Larger values can be noted in the north-western and north-eastern parts of the territory.

The fact that maps utilizing the Niemeğk observatory as reference station seem more detailed than ones constructed with the Surlari as reference station might be a result of the different structure beneath the two observatories. In the Surlari case, located in the study area, it can be supposed that the electric structure at large depths is relatively uniform (as also results from the MT model of the previous section, in which the mantle of various tectonic

units is characterized by the same resistivity value), and is probable that the electric properties in the observatory area have a larger weight, having as result the loss of some details.

A comparison with the electrical resistance obtained by the MT method (Fig. 2.1.2), even if both were constructed with values characterizing locations of the Secular Variation National Network stations (not shown), reveals rather important differences that derive from the two methods and from the distribution of information provided by the MT method. The latter refers to the central point of various squares of Fig. 2.1.1, and the stations of the Network could be located closer or far from that point, the attribution of an MT value being more or, respectively, less justified. The information given by the magnetic induction method is localized on the network station themselves. Also the depth range sounded by the two methods could be very different, the induction method treating it globally, while the MT method treats discrete depth ranges.

The L parameter, the inductance, is less intuitive than the resistance, and, consequently more difficult to interpret, having also in view the absence concerning this parameter in the scientific literature. L describes the degree of temporal delay of the Earth's response to variations of the magnetic inducing fields. In the presented maps one can note the existence of a low inductance NW-SE structure that separates areas with a comparatively higher inductance in the South-West and South from a North-East one.

Having in view that values obtained for R and L are the resultant of these properties for a rock column that contains both the crust and the upper mantle, in which several superposed conductive layers could exist, a more detailed interpretation is not possible for the moment. The density of the observation network is also prohibitive, being insufficient for revealing details at a finer scale, as was demonstrated by including four new stations.

2.2. Model of electric properties for Europe. Application of the magnetic induction model method

Introduction

The magnetic induction model, developed by the research team prior to the present contract and described in the previous section has been used in case of nine intense geomagnetic storms ($Dst < -150$ nT) occurred in the solar cycle 23, illustrated in Fig. 2.1.5 by the geomagnetic index Dst evolution. In the 2014 phase of the contract six days encompassing the storm were included. The results determined us to continue the investigation using only the main phase of the storm, with a duration of between 6 and 13 hours. We remind that for

this kind of study 1-minute recordings provided by the 29 European INTERMAGNET observatories.

The effect of the magnetospheric ring current was calculated for each observatory by means of:

$$\Delta_{Zs}^{Hs}(t) = \frac{\alpha_h}{\beta_h} \Delta He(t) + \frac{\alpha_z}{\beta_z} \Delta Ze(t)$$

$$He = \frac{M}{r^3} \cos \varphi = Dst \cdot \cos \varphi$$

$$Ze = \frac{2M}{r^3} \sin \varphi = 2Dst \cdot \sin \varphi$$

In which θ is the colatitude of the observation point, and the Dst index describes the effect of the magnetospheric ring current at the terrestrial magnetic equator.

Results

For each observatory the coefficients of the equation defining the magnetic induction model, the calculated values of the model and the corresponding residuals were derived.

The model residuals were then used, together with the time derivative of the recorded vertical component, to obtain the parameters L and R, the inductance and electric resistance for each observing point.

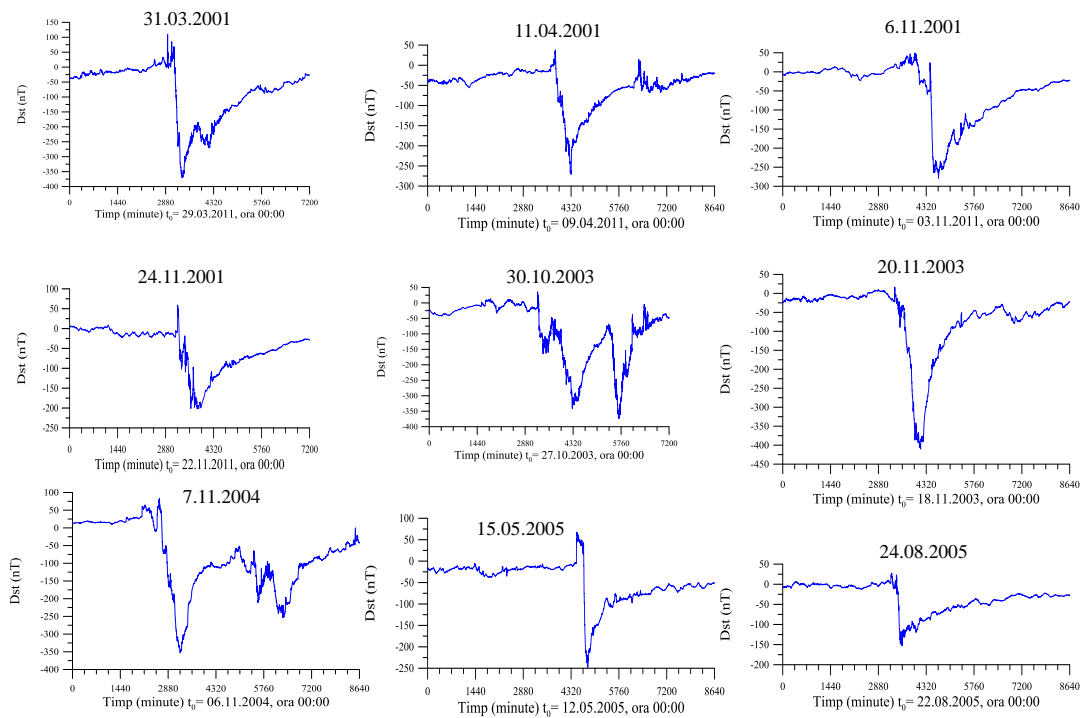


Figure 2.1.5. The nine geomagnetic storms of solar cycle 23 selected for the study

In Fig. 2.1.6 the results are presented as maps with normed values of the resistance R. Significant differences between the nine maps are evident. For the moment we have in view as a possible cause, on one hand, the different penetration depth of the electromagnetic signal produced by the storms, as the duration of the main phase, marked on the figure, and the different morphology of the storms main phase, on the other.

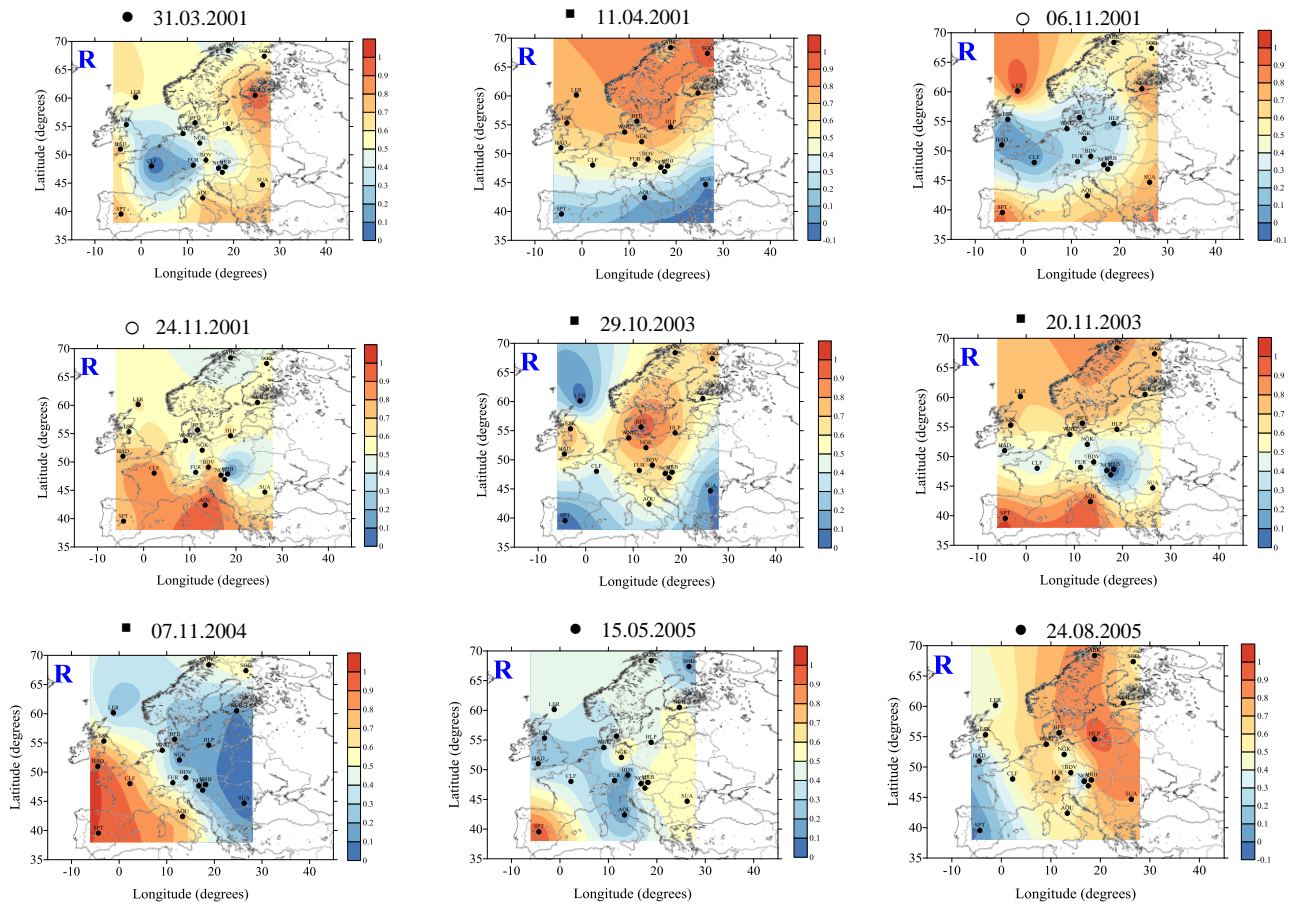


Figure 2.1.6. The geographical distribution of R for data from the main phase of the nine geomagnetic storms. Duration: ● 6 hours; ■ 10 hours; ○ 13 hours. Disturbing source: magnetospheric ring current

Though the magnetospheric ring current is, in general, the most important source of the magnetic disturbance at latitudes smaller than $\pm 60^\circ$, our research demonstrated that auroral electrojets could have significant effects, especially at high latitude observatories. The contribution of this source have been considered for the geomagnetic storm of May 15, 2005. The results for this storm are given in Figs. 2.1.7 and 2.1.8. The electric structure is compared to that given in Fig. 2.1.9, obtained using a synthesis of magnetotelluric data of the European project EURISGIC. The good accordance with the information based on magnetotelluric research indicates that in studies regarding geomagnetic and electric fields induced by magnetic storms the ionospheric auroral electrojets should be included as source.

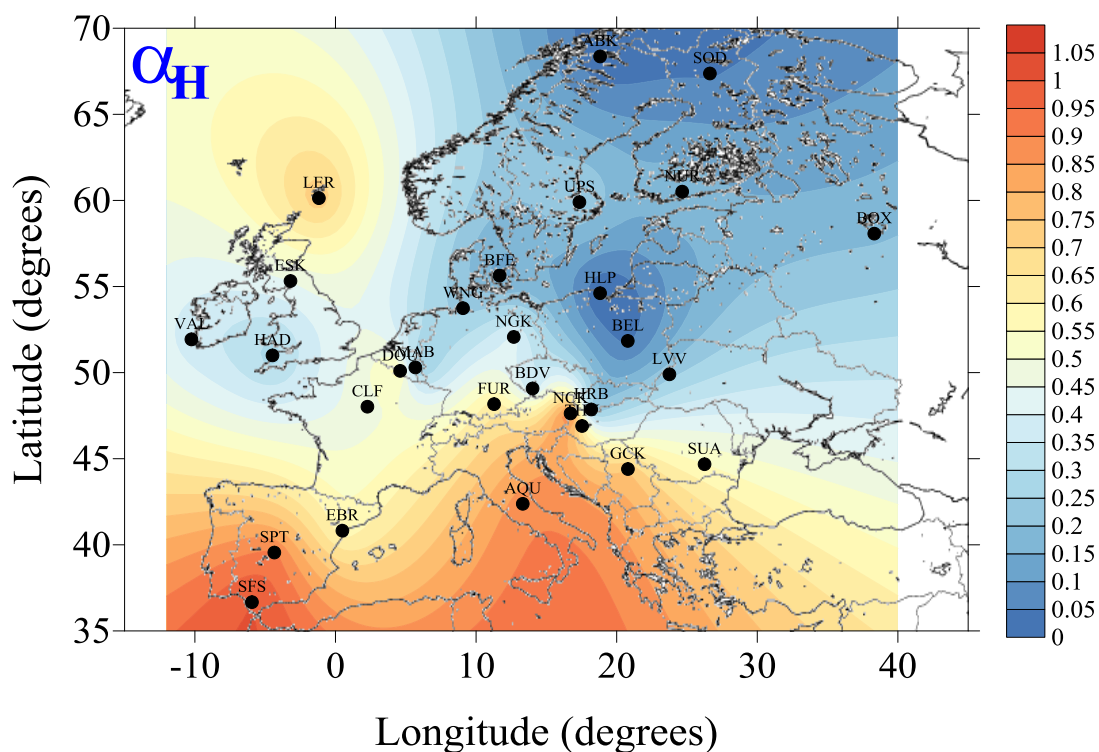


Figure 2.1.7. Image of the distribution of lithosphere magnetic properties, by the magnetic induction model for the storm of 15.05.2015. Disturbing sources: the magnetospheric ring current and the ionospheric auroral electrojet

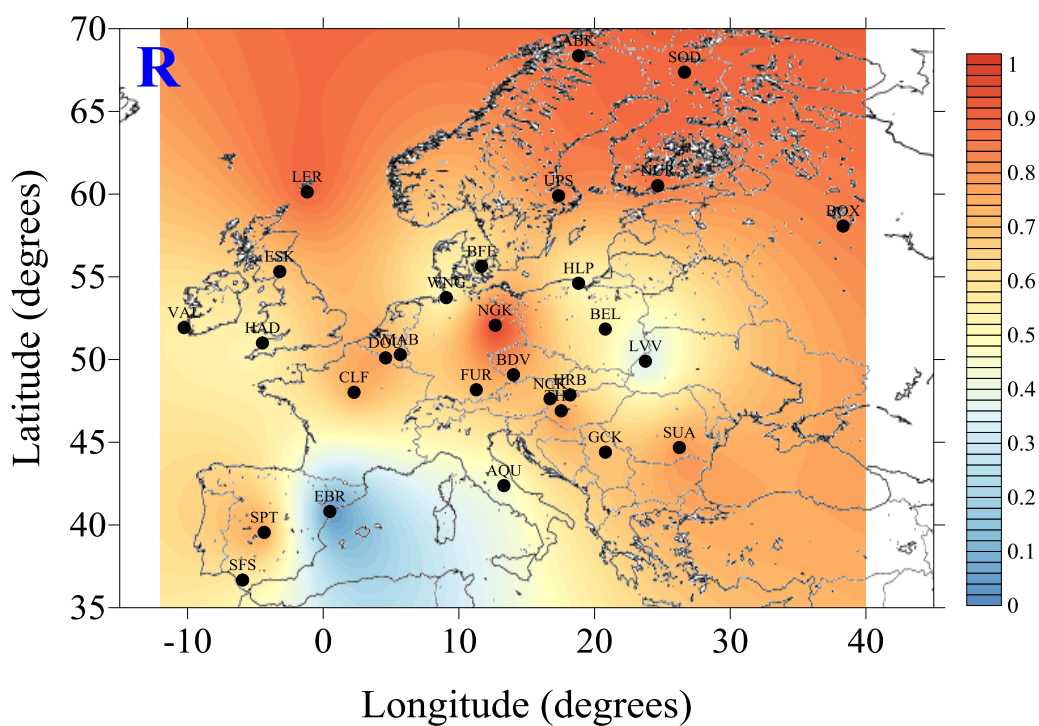


Figura 2.1.8. Image of the distribution of lithosphere electric resistance, by the magnetic induction model, for the storm of 15.05.2015. Disturbing source: the magnetospheric ring

The comparison with the results using the EURISGIC conductivities leads to a discussion of the same type as the above one for the Romania case, that takes into account both the distribution of information, localized in case of the magnetic induction model and distributed for large areas in the MT model, and the depth range investigated, the entire lithosphere as compared to the first 80 km.

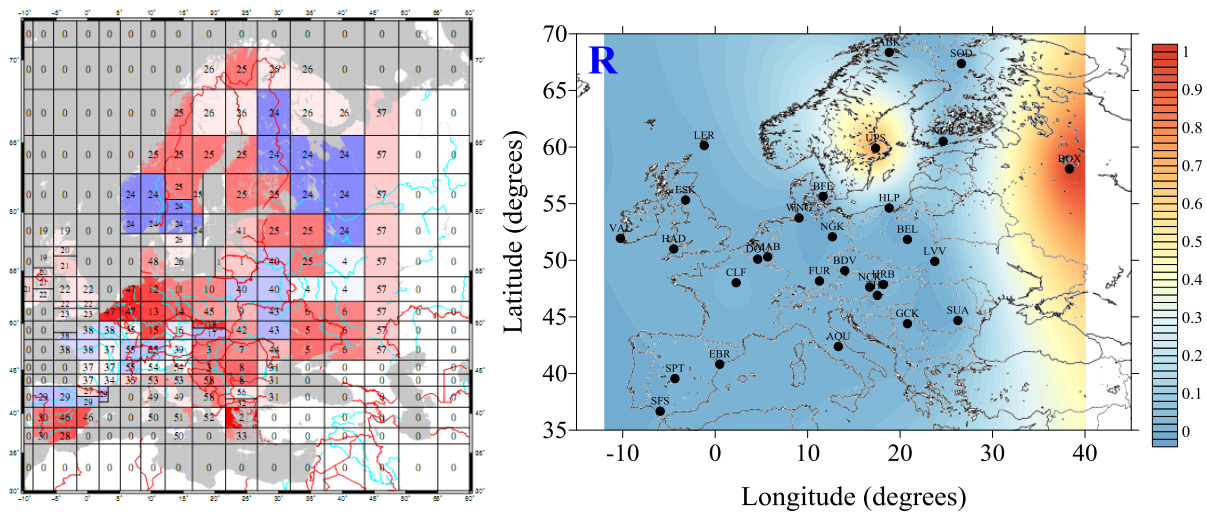


Figure 2.1.9. Electric properties of the lithosphere: the conductance for the first 80 km, published by the EURISGIC project (www.eurisgic.eu) (left) and the corresponding electric resistance as calculated for observatory coordinates (right)

References

- Cagniard, L., 1953, Basic theory of the magnetotelluric method of geophysical prospecting. *Geophysics*, 18, 605–635.
- Demetrescu, C., Andreescu, M., Ene, M., Neșțianu, T., 1985, Characteristics of the secular variation of the geomagnetic field between 1964 and 1981 in Romania, *Phys. Earth Planet Inter*, 37, 46-51.
- Demetrescu, C., Andreescu, M., Neșțianu, T., 1988, Induction model for the secular variation of the geomagnetic field in Europe, *Phys. Earth Planet. Inter.*, 50, 261-271.
- Demetrescu, C., Andreescu, M., 1992, Magnetic and electromagnetic induction effects in the annual means of geomagnetic elements, *NASA Technical Memorandum on “Types and Characteristics of Data for Geomagnetic Field Modelling”*, *NASA Conference Publication 3153*, 333-340.

- Demetrescu, C., Andreescu, M., 1994, Magnetic and electromagnetic induction effects in the annual means of the vertical component of the geomagnetic field at European Observatories, *Rev. Roum Géophysique*, 38, 73-84.
- Demetrescu, C., Dobrica, V., 2003, On the electric properties of rocks under the network of European geomagnetic observatories as derived from series of annual means of geomagnetic elements, *Rom. Rep. Phys.*, 55, 411-420.
- Dobrica, V., Mogi, T., Demetrescu, C., Takada, M., 2008-2009, Magnetic induction effects of the diurnal variation. Case study – the Hokkaido magnetometric array. *Rev. Roum. Geophys.*, 52-53, 33-47.
- Stănică, D., Stănică, M., 1993, An electrical resistivity lithospheric model in the Carpathian Orogen from Romania. *Physics of the Earth and Planetary Interiors, Crustal - Scale Studies*, 81, 99-105.
- Săndulescu, M., Visarion, M., Stănică, D., Stănică, M., Atnasiu, L., 1993, Deep structure of the Inner Carpathians in the Maramures-Tisa Zone (East Carpathians). *Rom. J. Geophys.*, 6, 67-76.
- Stănică, M., Stănică, D., 1996, Magnetotelluric studies in the Tethian Suture Zone on the Pannono-Carpathian Geotranssect. *Rev. Roum. Geophys.*, 40, 71-80.
- Stănică, D., Stănică, M., Balea, Al., Ivanov, A., 1996a, Studies by magnetotelluric soundings in new and prospective zones having genetic conditions favourable for the accumulation of the metalliferous ore deposits-Baia Mare zone (Coas-Firiza Valley profile). *Anuarul IGR*, 69, Partea I, 280-282.
- Stănică, D., Stănică, M., Asimopolos, L., Ivanov, A., Nistor, H., Visarion, C., 1996b, Studies by magnetotelluric soundings in new and prospective zones having genetic conditions favourable to the accumulations of mineral metalliferous resources in Baia Mare zone. *Anuarul IGR*, 69, Partea I, 277-279.
- Stănică, M., Stănică, D., Asimopolos, L., Ivanov, A., Nistor, H., 1997, Magnetotelluric researches along Lugoj-Teregova and Alba Iulia-Agnita profiles, *Anuarul IGR*, 70, 11-25.
- Stănică, D., Stănică, M., 1998, 2 D modelling of the geoelectrical structure in the area of the deep-focus Vrancea Earthquakes. *Monography of Southern Carpathians, Reports on Geodesy*, 7, 193-203.
- Stănică, M., Stănică, D., Marin-Furnica, C., 1999, The placement of the Trans-European Suture Zone by electromagnetic arguments on the Romanian territory. *Earth, Planets and Space*, 51, 1073-1078.

Stănică, D., Stănică, M., Piccardi, L., Tondi, E., Cell, G., 2004, Evidence of geodynamic torsion in the Vrancea zone (Eastern Carpathians), *Rev. Roum. de Geophysique*, 48, 15-21.

Tikhonov, A. N., 1950, The determination of the electrical properties of deep layers of the Earth's crust. *Dokl Acad Nauk SSR*, 73, 295–297 (in Russian).

Chapter III. The analysis of solar eruptive processes and solar wind, responsible for risk geomagnetic activity (geomagnetic storms and substorms) during 1964-2014

3.1. Introduction

The influence of solar eruptive processes on Earth represents a high-end subject in the context generated by satellite missions which study the Sun, and also the heliosphere. Solar observations have progressed tremendously since the first studies regarding eruptive processes followed by geomagnetic storms (Carrington, 1859; Hogson, 1859), having reached today to solar disk images in a large number of wavelengths, magnetic configuration images of the Sun, as well as many other parameters measurements nearby Earth, which allow evaluating of interplanetary magnetic field (heliospheric) conditions, obtaining information on the particle flux arriving at Earth (solar wind) and last, but not least, estimating of magnetospheric and ionospheric sources which perturb the terrestrial magnetic field produced in our planet's outer core. From the various solar eruptive processes, the research team focused during the present project on coronal mass ejections (CMEs), which have a direct impact on the magnetosphere when they propagate towards Earth. Also, in the research frame of the current project, high speed streams from the solar wind had an important weight. Both subjects contributed to determining some essential characteristics of triggering the risk geomagnetic activity, recorded at Earth's surface as geomagnetic storms and substorms. Geomagnetic variability leads to the appearance of geomagnetically induced currents (GICs) which affect the proper functioning of high voltage electrical networks, of transoceanic cables, of vastly spread oil pipes and of electric railroads (Maris and Crosby, 2012). The results regarding GICs are presented in the next chapter of the current report.

3.2. Coronal mass ejections

Coronal mass ejections are huge quantities of magnetized plasma expelled from the Sun's atmosphere out into the interplanetary space. The ejections observed in the interplanetary space are also known as interplanetary coronal mass ejections (ICMEs). When these ICMEs interact with Earth's magnetosphere, they can produce major geomagnetic disturbances known as geomagnetic storms. They are characterized by significant variations of aa, Dst and AE indices supplied by the Geomagnetic Data World Centre from Kyoto, based on geomagnetic field recordings from various geomagnetic ground-based observatories.

In order to determine the characteristic ejection parameters we used reconstruction techniques such as triangulation, polarization ratio, direct modelling (see e.g. Mierla et al.,

2008; 2009; 2010; 2011). The speeds determined with these techniques were compared with the speeds measured in-situ (by ACE and WIND), in order to improve the methods of time propagation prognosis of CMEs from Sun to Earth (Oprea et al., 2012). It was noticed that the CMEs initial speed and the interplanetary magnetic field component Bz play an important role in producing major geomagnetic storms (Srivastava and Venkatakrishnan, 2004).

In the frame of the present contract, we studied in detail the CMEs produced during solar cycle 23 (1996 – 2008), for which there are systematic data, the ones that triggered major storms (characterized by geomagnetic index $Dst < -150$ nT), as well as those that produced moderate storms ($-150 < Dst < -50$ nT).

3.2.1. Analysis of CMEs responsible for risk geomagnetic activity (storms with $Dst < -150$ nT) during solar cycle 23

The obtained results are thoroughly presented and discussed in the stage 2014 report of the current project. A first step of the research was the selection of storms which were associated with ICMEs (Richardson and Cane, 2010; Zhang et al., 2007); we synthesized the main characteristics of ejections that triggered the selected geomagnetic storms and we present them in Table 1.

Table 1: General properties of geo-effective coronal ejections with $Dst < -150$ nT.

CME	Position	V_{linear} (km/s)	2 nd order V at final height (km/s)	2 nd order V at 20 Rs (km/s)	Accelera tion (m/s^2)	$V_{transit}$ at 1 AU (km/s)
1998/05/02 – 14:06:12 H	S17W24	938	697	871	-28.8	1150
1998/05/02 – 05:31:56 H	S17W24	542	527	530	-1.4	--
1998/05/01 – 23:40:09 H	S16W12	585	657	627	8	--
1998/04/29 – 16:58:54 H	--	1374	1151	1250	-44.8	--
1998/08/24 – 21:50	N35E09	--	--	--	--	1260
1998/09/23 – 06:40	N18E09	--	--	--	--	1020
1999/09/20 – 06:06:05 H	S20E01	604	549	357	-14.5	770
1999/10/18 – 00:06:06 PH	S26E08	144	263	290	3.5	561
2000/04/04 – 16:32:37 H	N18W72	1188	1232	1199	12.8	860
2000/07/14 – 10:54:07 H	N17W11	1674	1534	1147	-96.1	1500
2000/08/09 – 16:30:05 H	N11W15	703	731	720	2.8	830
2000/09/16 – 05:18:14 H	N14W07	1215	1162	1192	-12.3	--
2000/09/15 – 21:50:07 H	--	257	285	537	11.2	--

2000/09/15 – 15:26:05 PH	N13W00	481	370	335	-10.4	--
2000/09/15 – 12:06:05 PH	N13W00	633	395	0	-64	--
2000/10/02 – 20:26:05 H	S09E04	569	478	483	7.1	756
2000/11/03 – 18:26:06 H	N23W71	291	475	643	16.4	660
2001/03/28 – 12:50:05 H	N17W03	519	582	561	4.4	690
2001/03/29 – 10:26:05 H	N13W14	942	965	957	3.5	--
2001/04/10 – 05:30:00 H	S22W20	2411	2876	2974	211.6	1290
2001/04/09 – 15:54:02 H	S21W08	1192	1198	1198	1.3	--
2001/09/29 – 11:54:05 PH	N14W01	509	470	150	-12	715
2001/10/19 – 16:50:05 H	S14W62	901	895	898	-0.7	870
2001/10/25 – 15:26:05 H	S19W26	1092	1080	1087	-1.4	694
2001/10/24 – 06:26:05	S12E14	597	633	653	4.6	--
2001/11/04 – 16:35:06 H	N05W29	1810	1514	1691	-63.4	1250
2001/11/03 – 19:20:05 H	N06W14	457	329	299	-9.9	--
2001/11/22 – 23:30:05 H	S18W24	1437	1371	1409	-12.9	1320
2002/09/05 – 16:54:06 H	--	1748	1855	1903	43	880
2002/09/26 – 01:31:44 PH	--	178	368	331	5.1	--
2003/10/28 – 11:30:05 H	S16E04	2459	2229	2268	-105.2	2185
2003/10/29 – 20:54:05 H	S17W10	2029	1670	1519	-146.5	2138
2003/11/18 – 08:50:05 H	N03E08	1660	1645	1656	-3.3	886
2004/07/25 – 14:54:05 H	N08E35	1333	1366	1359	7	1302
2004/11/04 – 23:30:05 PH	--	1055	1037	1050	-1.9	720
2004/11/04 – 09:54:05 H	N09E32	653	719	706	6.3	--
2004/11/07 – 16:54:05 H	N09E08	1759	1696	1713	-19.7	830
2004/11/06 – 02:06:05 PH	N09E06	1111	1258	1176	18.8	
2005/05/13 – 17:12:05 H	N12E05	1689	--	--	--	1270
2005/08/22 – 01:31:48 H	S11W54	1194	1086	1127	-17.8	790
2005/08/22 – 17:30:05 H	S13W65	2378	2612	2585	108	
2006/12/13 – 02:54:04 H	-	1774	1622	1573	-61.4	1180

The analysed coronal mass ejections are mostly Halo (angular width greater than 120°), as seen in LASCO/SOHO white light images (e. g. Fig. 3.1).

Only 18 ejections have positive acceleration values, which mean that most of them are slowed down after being expelled from the Sun's vicinity. For an accurate acceleration measurement, but mostly to better determine the time and height variation, one needs data from the low corona. Studies of St. Cyr et al. (1999) and Zhang et al. (2001) show that the

acceleration has the highest value in the lower corona and there is no deceleration below 3 solar radii, despite gravity. 30% of the ejections seen by LASCO/SOHO are slowed down, percentage which rises up to 54% in the case of our selected events.

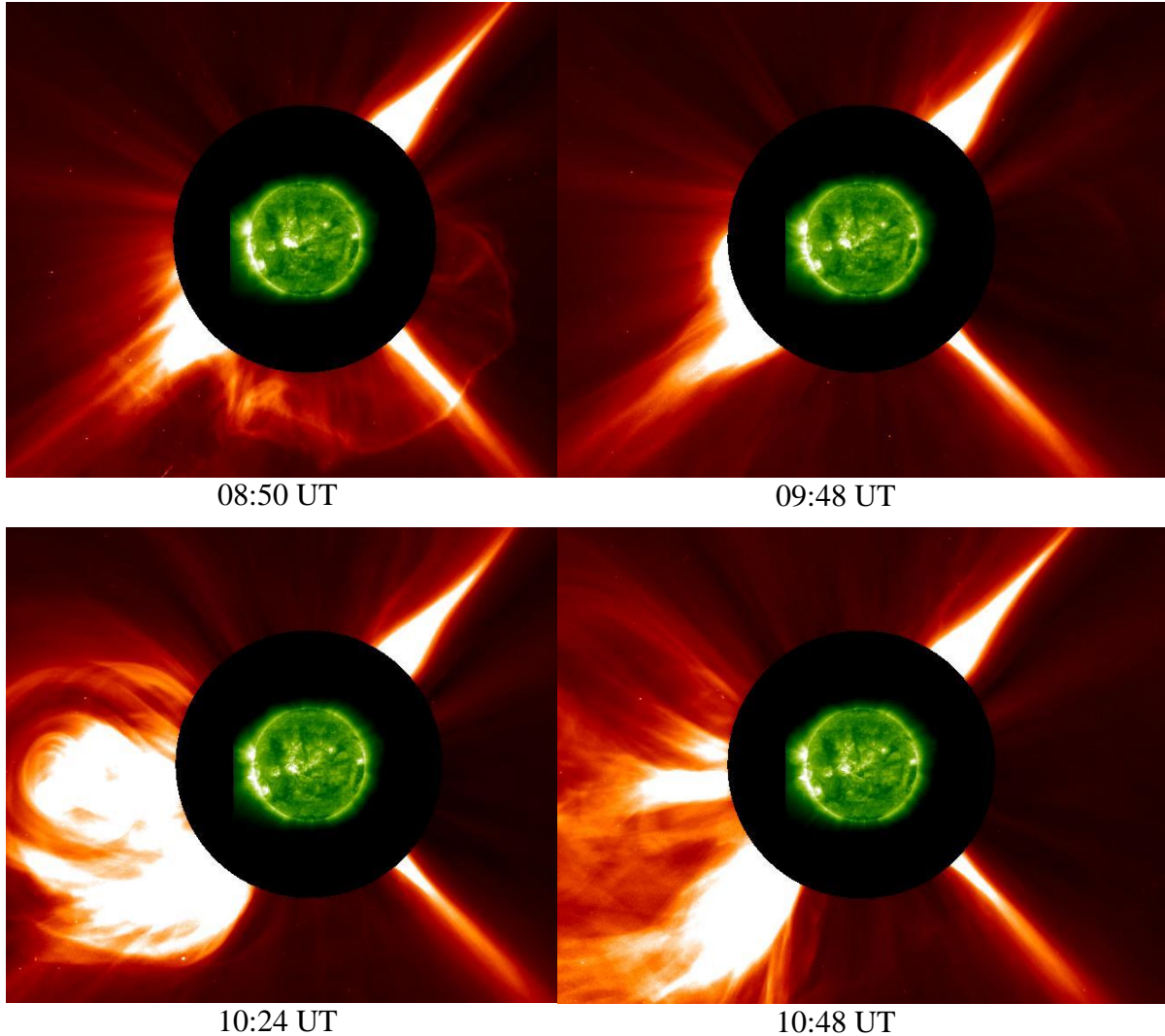


Figure 3.1. The evolution of a coronal mass ejection on 18 November 2003. LASCO C2 images selection overlapped with solar disk images in 195 Å, provided by EIT. Images created in Jhelioviewer (jhelioviewer.org/).

Following the analysis, we concluded that geo-effectiveness depends greatly on the solar disk location of the ejections, which is included in a rectangle bordered by -35° and 72° longitude and 35° and -26° latitude.

The statistic evaluation of the geo-effective CMEs number was not significant in this case, due to the large number of ejections detected by LASCO (at maximum solar activity there can be several ejections a day) and the much lower number of geomagnetic storms; therefore, the probability for a certain eruptive phenomenon to be geo-effective was

evaluated. A coronal mass ejection whose speed is not the largest, but overlaps an interplanetary magnetic field line oriented southwards, will be more geo-effective than a stronger coronal ejection which does not reach Earth during the negative Bz.

In a second step of the research, three events were analysed and described in detail, namely the CMEs on 18.11.2003, 7.11.2004 and 22.08.2005. The first one, seen in Fig. 3.1, triggered the strongest storm from solar cycle 23, having a Dst = -422 nT, storm which we analysed in the next chapter from the GIC point of view.

All remarkable storms from cycle 23 took place during the maximum phase of the cycle, therefore particle fluxes emitted by solar eruptive phenomena possess a main role in triggering geomagnetic storms. If these fluxes presented HSS characteristics, they were also synthesized. The results emphasized the absence of a direct or one-to-one correlation between the CME characteristic parameters and the geomagnetic storms magnitude. It was also concluded that magnetic field orientation is important and must be southward oriented (negative Bz) in order to allow reconnections which lead to energy transfer to the magnetosphere.

3.2.2. Analysis of CMEs/ICMEs responsible for moderate geomagnetic activity (storms with $-150 \text{ nT} < \text{Dst} < -50 \text{ nT}$) from solar cycle 23

During the minimum, ascending and maximum phases of solar cycle 23 there were 97 moderate geomagnetic storms recorded which were triggered by ICMEs, out of which 61 were associated with coronal mass ejections. In the 2014 stage report there were 56 events analysed, for which there is a clear association between the geomagnetic storm, ICME and CME. For the identification of this set of events the Richardson and Cane (2010) catalogue was used (available and updated on-line), and also data from LASCO (Large Angle and Spectrometric Coronagraph) CME catalogue, available at http://cdaw.gsfc.nasa.gov/CME_list/. LASCO catalogue is based on data provided by SOHO (Solar and Heliospheric Observatory) mission, namely white light images from LASCO instrument (Brueckner et al. 1995), on IMP 8, Geotail, Wind and ACE data, provided through OMNIWEB interface (<http://omniweb.gsfc.nasa.gov>), maintained by Goddard Space Flight Center – NASA, and on final Dst index values provided by Kyoto University.

In the present study we considered as representative for the 56 selected coronal mass ejections the following parameters: date and hour at which the ejection was detected by LASCO, solar disk location, linear speed, velocity at final height and at 20 solar radii ($\sim 1,39 \times$

10^7 km), acceleration, as well as the ICME speed recorded at one astronomical unit ($\sim 1.49 \times 10^8$ km).

Ejection speed evolution in the interplanetary space presents the following aspects. There are 27 CMEs ($\sim 48\%$) whose speeds increase in value from the distance of 20 solar radii to one astronomical unit, percentage which differs from its equivalent for coronal mass ejections triggering major geomagnetic storms, and that is now below 25%. The other 52% ejections were decelerated due to the interaction with the solar wind. Approximately half of the considered coronal ejections (25 ejections) are slowed down after being expelled from the Sun's vicinity, a similar result with that of the ejections triggering intense geomagnetic storms. For an accurate measurement of acceleration, but mostly for the time and height variation, data from the low corona are needed. In this case too we found the results of St. Cyr et al. (1999) and Zhang et al. (2001).

The coronal ejections sources are delimited by a rectangle enclosed between -35° and 72° longitude and 23° and -22° latitude, a narrower area than the one obtained in the previous study (section 3.2.1) which referred to ejections that triggered major geomagnetic storms.

The coronal mass ejection with the highest speeds – 2505 km/s linear speed and 2827 km/s speed at final height – took place on the 2nd of April 2001. The transit velocity associated with this event was 1020 km/s, which is not the largest value of all the considered events. The highest transit speed was the one associated to the event on 22 May 2002, with a value of 1323 km/s.

3.3. High speed streams in the solar wind

The solar wind (SW), a continuum plasma flux coming from the solar corona, is a heterogeneous environment structured by different parameters (density, plasma speed, heliospheric magnetic field structure). The solar wind has two components: slow SW and fast SW (made of high speed streams – HSS). The slow solar wind is characterized by speeds of approximately 300 – 350 km/s, temperature of $0.4 - 1.6 \times 10^5$ K and a chemical composition similar to that of the solar corona. The fast SW (HSS) has speeds between 500 – 750 km/s (even exceeding 1000 km/s), temperatures around 8×10^5 K and the chemical composition is similar to the solar photosphere. The sources of HSS from the solar corona are coronal holes (CH), open magnetic field structures which appear in the polar regions at maximum solar activity and stretch as low as medium and equatorial latitudes during solar minimum. At the impact with the magnetosphere, HSS produce medium intensity geomagnetic perturbations, but in some favourable conditions (overlapping the interplanetary space with a sectorial

border, the interaction with an ICME), they can also produce important geomagnetic storms. Their geo-effectiveness is directly dependent on the solar source – coronal hole – being mainly influenced by its heliographic position. Therefore, it is possible for a CH from the equatorial area or with large equatorial extensions to produce HSS with major effect in the magnetosphere. Such coronal holes are mostly seen during minimum solar activity or at the end of descending phase. Also, HSS emitted by CH are more geo-effective when CH are closer to the central meridian of the Sun and while passing through the western hemisphere. The solar wind plays an important role for the structure and dynamics of the heliosphere, because the magnetised solar plasma structures the medium through which it propagates. A HSS that propagates from the solar corona to the interplanetary space interacts with the slow solar wind resulting at the border between the two regimes of flow, a compression region named co-rotating interaction region (CIR) which often is maintained during several solar rotations. These structures appear because the plasma is frozen in the magnetic field such as the two currents (fast and slow) do not mix, but form a persistent interface at their confluence area. Plasma properties of the solar wind and the structure of the interplanetary magnetic field differ from one another in the two regions separated by the interface.

3.3.1. HSS Catalogue. HSS dynamics for the last four solar cycles (1984 – 2008)

There are many HSS definitions, but the generally accepted one is taken from the first catalogues of Lindblad and Lundstedt (1981; 1983; 1989): HSS is considered to be a plasma flux with high speed in the solar wind, lasting for several days. The selection criterion of these currents was $\Delta V1 \geq 100 \text{ km/s}$, where $\Delta V1$ is the difference between the smallest speed value for the 3-h interval in a given day ($V0$) and the largest speed value for the 3-h interval in the next day ($V1$); this difference must last at least two days. There are currents that last 2-3 days, but there are also long duration currents (over 5-6 days). The larger the maximum speed, the larger the particle energy is, and the current has a greater geophysical efficiency. Obviously, the largest maximum speeds are registered during HSS produced by solar eruptive phenomena.

Mavromichalaki et al. (1988; 1998) continued the identification of solar wind currents and published results for solar cycle 22. For solar cycle 23 (1996-2008) the HSS Catalogue was elaborated in three stages for the PN2 HELIOTER project, 2007-2010 (Mariş and Mariş, 2009; 2011). An HSS catalogue for 1996-2007 was elaborated by an Indian scientific team (Gupta and Badruddin, 2010). Therefore, there are HSS catalogues for four solar cycles (no.

20-23), that cover the 1964-2008 time interval. In the present contract HSS identification was continued for solar cycle 24.

In order to correctly evaluate the **intensity** of a current or its **importance** – in its efficiency of producing geophysical effects – the I parameter is used (called **importance** or intensity of an HSS) defined as $I = \Delta V_{max} \times d$, for which we can calculate its weighted value taking into account the duration of each HSS, as well as their frequency.

In the frame of the present contract we analysed the dynamics of the monthly values of the HSS importance parameter (ΣI), separately for HSS produced by CH (CH_HSS) and those produced by solar eruptive events (FG_HSS), during the four solar cycles, no. 20-23. It is easily seen that the two types of HSS (produced by CH and solar eruptive events) present an anti-phase variation (Fig. 3.2). Thus HSS produced by CH have ΣI maxima with 2-3 years before the solar cycle maxima, unlike the maxima for ΣI for HSS produced by solar eruptive events, that appear in the maximum phase of the solar cycle (Fig. 3.3). Also noteworthy was the anti-phase variation of A_p and I in certain intervals of solar cycle 22, as well as in the minimum period between solar cycles 23 and 24.

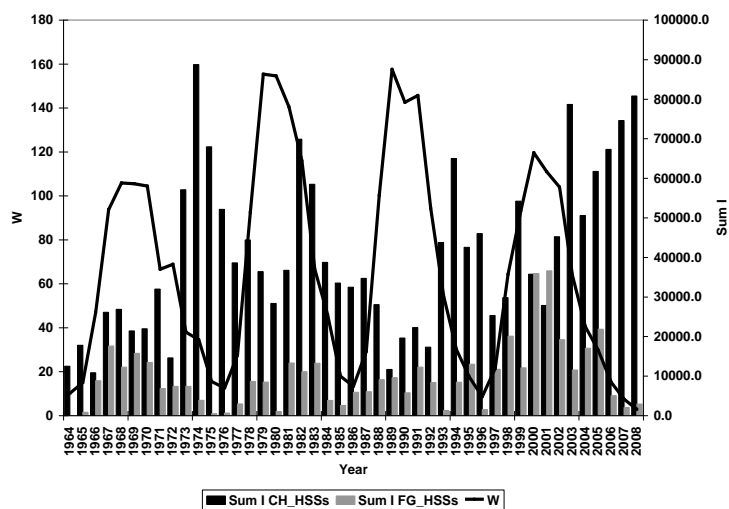


Figure 3.2. Dynamics of the monthly values of HSS importance (ΣI), shown separately for HSS produced by CH (CH_HSS) and by solar eruptive events (FG_HSS), during four solar cycles no. 20 – 23 (Maris and Maris, 2012)

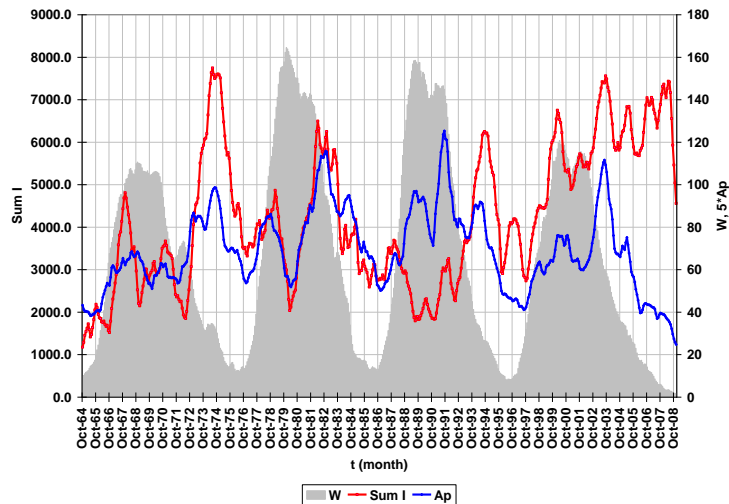


Figure 3.3. I and Ap variation (monthly smoothed values) compared to monthly smoothed values of Wolf number (W), during four solar cycles (1964 – 2008) (Mariş et al., 2011).

The geomagnetic effects are stronger in the case that two fast currents of solar wind (SW), with different solar sources, arrive at Earth in intervals of the order of hour or day, but the Bz component can favour or restrict magnetic reconnections that would permit an efficient energy transfer.

3.3.2. HSS contribution to moderate geomagnetic activity during solar cycle 23

This study referred to the currents in solar wind produced by coronal holes and geomagnetic storms produced by the HSS impact to the terrestrial magnetosphere. We used data concerning HSS that were listed in the HSS Catalogue (Maris and Maris, 2012) for solar cycle 23, 1996-2008. In this study we took into consideration the moderate geomagnetic storms ($-100 \leq Dst \leq -50$ nT) and the intense storms ($Dst \leq -100$), where we used the “Complex Catalogue HSS_GS” (Maris and Maris, 2010), drawing up a table with currents list that were produced by coronal holes and have triggered geomagnetic storms, presented in the 2014 stage of the contract. In Figures 3.4 and 3.5 there are the HSS/geomagnetic storms statistics, for solar cycle 23 (annual number, respectively statistics from the viewpoint of the geomagnetic storm intensity). It can be seen that these currents are not uniformly distributed across the solar cycle 23. It was concluded that at minimum activity (year 1996), HSS were able to produce more geomagnetic storms because of the currents solar source – coronal holes. It is also observed the intensification of the HSS produced in the year next to the polarity change in the solar magnetic field (2001), as well as the sustained activity maintaining of the HSS during the descending phase of the cycle.

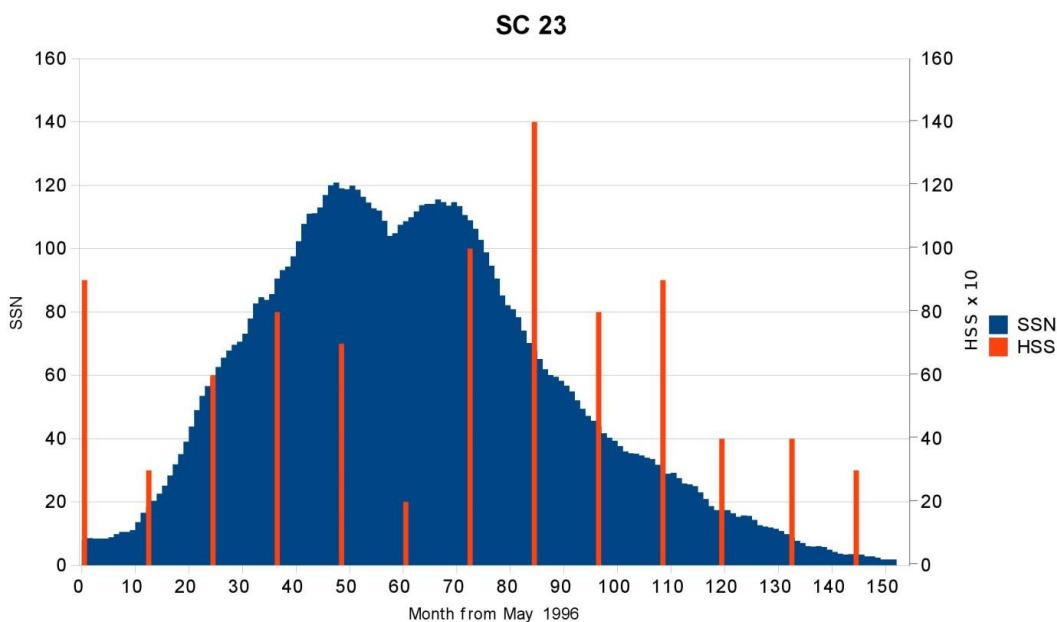


Figure 3.4. Annual number histogram of HSS that produced geomagnetic storms in SC 23. Background – monthly smoothed mean values of the sunspot number (SSN).

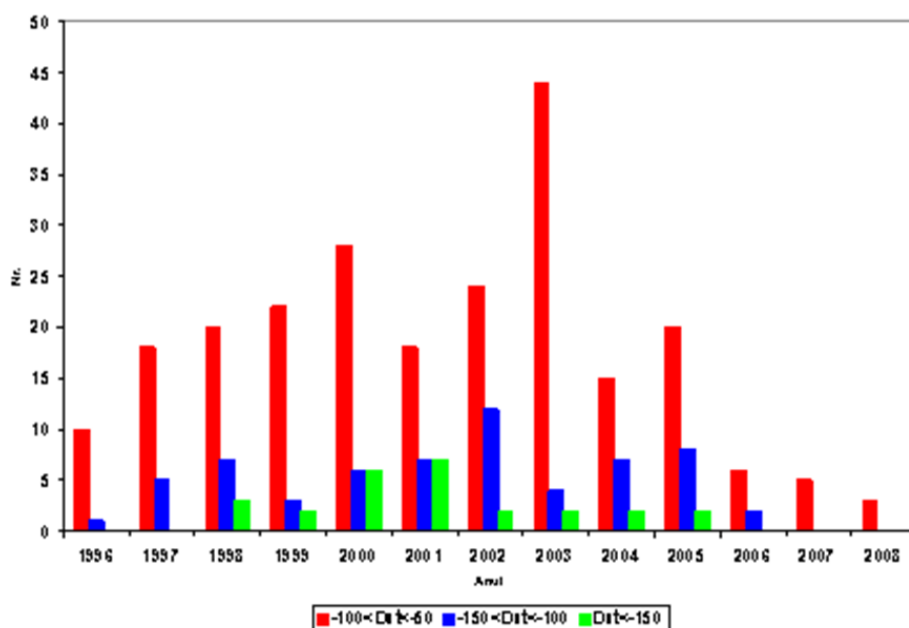


Figure 3.5. Annual distribution of the geomagnetic storms in SC23 produced by HSS, with respect to intensity (Maris & Maris, 2010, Complex Catalogue: GSs-HSSs, 1996 – 2008; http://www.space.ro/new1/GS_HSS_Catalogue.html)

Some characteristics of the HSS and storms from SC23 produced by the interaction of the HSS with magnetosphere are synthesised in each year of the cycle in Table 3.2.

Table 3.2. Characteristics of the analysed HSS and storms

	1996	1997	1998	1999	2000	2001	2002	2003	2004	2005	2006	2007	2008
No. HSS	9	3	6	8	7	2	10	14	8	9	4	4	3
VMax >600km/s	7	-	3	4	2	1	7	10	4	8	3	3	2
DVmax >300km/s	1	-	-	4	-	1	6	5	2	7	3	3	2
Dst< -100	1	-	1	-	-	-	4	1	-	1	-	-	-
SSC	1	2	2	7	1	2	2	-	3	3	1	2	2

HSS geoeffectiveness can be synthesised in a few conclusions: HSS emitted from coronal holes situated in the eastern solar hemisphere, do not perturb the terrestrial magnetosphere; the position of the coronal hole near the central meridian ($\pm 10^\circ$) of the solar disk ensures an HSS geoeffectiveness of approximately 60%; coronal holes situated in the western hemisphere produce HSS with high geoeffectiveness, up to 98%; the compact structure and the extended surface of the coronal hole can contribute to the HSS energy, that may increase its geoeffectiveness.

We also synthesised the data concerning the minimum Dst value, Bz min and the interval during which Bz remains negative before, and near the Dst min moment: the interval between Bz and Dst min is 1-3 hours, with little exception in which the duration increases to 4 or even 5 hours; Bz remains negative during many hours, over 5 in most cases (90 %), which ensures an efficient energy transfer; only 8% of the geomagnetic storms are intense and to these we can observe the persistence of negative Bz for a longer period (≥ 8 hours); negative Bz ensures a higher geo-efficiency of an HSS than the speed (energy) of its particles. It was concluded that the registration of an increase in solar wind plasma (an HSS) at ACE (Lagrangian point L1) and the concomitant analysis of Bz values, make the prognosis of a geomagnetic storm possible with at least 2 hours ahead of its beginning.

3.4. On the geoeffectiveness of solar and heliospheric processes. Correlation analysis for various pairs of variables characteristic to CMEs, HSSs and geomagnetic storms

The propagation of a high speed stream in solar wind over a sector border significantly increases the solar plasma effectivity in perturbing the terrestrial magnetosphere. Amongst the analysed phenomena in solar cycle 23, HSS from 28 may 2005, that has a speed increase of only 255.4 km/s, was distinguished by a significant increase in plasma density (by 50-100%), comparative with other events of the same month. This increase could be explained by the collision of the inclined current sheet with HSS plasma particles (Eselevich and Fainshtein, 1991). The variability of the heliospheric magnetic field (HMF) sign induced the relatively large value of B_z (-16.1 nT), which permitted an efficient reconnection and an intense geomagnetic storm.

The geoeffectiveness of solar phenomena depends on two essential factors: phenomenon energy and propagation direction from the Sun towards the Earth. The energy of some eruptive phenomena is directly dependent to the solar source, its localisation in the solar atmospheric layers, the source magnetic structure and the expulsion speed of the solar (plasma) particles. The propagation direction is influenced by the source phenomenon position on the solar disk and the particle fascicle width during propagation (most efficient CMEs being the Halo ones, or with angular width larger than 120°). The geoeffectiveness of a complex event can significantly increase or it can be sensibly diminished as a function of the magnetic structure of the plasma that leaves from the solar sources and interact during the propagation. The essential role in geoeffectiveness is played by the B_z component of the interplanetary magnetic field.

The study realised for the maximum phase of cycle 23 (Oprea et al., 2012) for major geomagnetic storms ($Dst \leq -200$ nT) and for intense geomagnetic storms ($Dst \leq -100$ nT) showed the following observations regarding the solar phenomena geoeffectiveness: the combination of complex sources (CIR and ICME or flares and ejections) induces significant negative values of Dst and their maintaining during a couple of hours; the energy entered in magnetosphere, estimated using the Akasofu parameter, is proportional to the plasma speed, but also with the heliospheric field intensity, and the duration of the reconnection depends of the duration while B_z remains negative; solar eruptive events that come from different sources, with different magnetic structures, determines the complex main phase of the geomagnetic storm.

During this contract we also performed detailed correlation studies between CMEs characteristic variable couples (linear speed variation of the CME), the heliospheric magnetic field (B_z) and the geomagnetic storm intensity (Dst index). Table 3.3 presents the determination coefficient R^2 referring to our analysed selection of events.

Table 3.3: R^2 coefficient values

Cycle phase 23	(Vcme, Dst)	(Vcme*Bz, Dst)	(Ek, Dst)
Minimum and ascending	0.0035	0.1425	0.0162
Maximum	0.1481	0.0773	0.1145

The results concerning the analysis of the Dst values dispersion compared to $V*Bz$ product suggests that the geomagnetic efficiency must take into account this product.

The same detailed analysis was also performed for the connection between the high speed currents from solar wind (HSS) and their effects in magnetosphere (geomagnetic storms). The correlation analysis is synthesised in Table 3.6 through the means of determination coefficient R^2 for various pairs of HSS characteristic values and geomagnetic storms.

For all three phases of the solar cycle 23, it was seen that the effect of the maximum speed and the HSS gradient speed practically does not exist in the Dst variation (R^2 values between 0.001 – 0.0425). It was also seen higher R^2 values for the combined effect of V_{max} and Bz in the product of $V_{max}*Bz$, in comparison with $\Delta V_{max}*Bz$ product effect in the Dst variation.

In this stage the geomagnetic efficiency modelling was based on observations referring to relations between certain ejection properties and triggering of the geomagnetic storms. The coronal mass ejection that produced the strongest geomagnetic storm from the present event selection was that of 17 April 2002, a halo type one, with linear speed of 1240 km/s, therefore a fast ejection. At the opposite end, the least effective ejection is also the fastest from this selection, that from 2 April 2001, with a linear speed of 2505 km/s. The position of the first CME on the solar disk was S14W34, while for the second one was N15W60, thus confirming previous studies (Zhang et al., 2007) concerning CME efficiency as a function of their position such as: locations situated at higher latitudes are less likely to be geo-effective because they will propagate at higher latitudes in heliosphere and will not reach Earth.

Table 3.4 synthesises correlation results between selected parameters and Dst, as depending on the solar cycle phase.

Table 3.4: Determination coefficient (R^2) of Bz and projected speed of the CME with Dst variations during various phases of SC 23

	Minimum and Ascending Phase	Maximum Phase	Descending Phase	SC23
$R^2(B_z, Dst)$	0.21	0.45	0.38	0.29
$R^2(V_{cme}, Dst)$	0.00	0.15	0.00	0.03
$R^2(B_z * V_{cme}, Dst)$	0.14	0.14	0.21	0.09

For modelling the geomagnetic efficiency of the eruptive solar processes we chose a model proposed by Srivastava (2005) – a model that expresses the probability that a certain coronal mass ejection to be followed by a severe geomagnetic storm described by a geomagnetic index $Dst < -150$ nT – and modified as requested. The model is based on the logistic regression method applied to an independent variables series of solar and interplanetary parameters, as well as a dependent variable – the geomagnetic index Dst.

The novelty of this study consists of introducing two variations of this model such as: a version that kept the variable number – 9 – but only CME characteristic parameters; another version that increased the number of variables – 11 – but kept the two interplanetary space characteristic measures (B and Bz). By means of a modified version (Besliu-Ionescu et al., 2016) we managed to obtain probabilities of moderate geomagnetic storm triggering on a selection of 68 events out of the 81 events for which we could establish a correct “chain”: coronal mass ejection – interplanetary coronal mass ejection – geomagnetic storms. These coefficients are listed in Table 3.5.

Table 3.5. Coefficients resulting after applying the logistic regression model.

	Value of the regression coefficient – 9 variables	Value of the regression coefficient – 9 variables	Value of the regression coefficient – 11 variables
(b ₀)	8.2097	8.2217	8.2186
Projected CME speed (b ₁)	1.34E-06	7.59E-06	-3.65E-07
CME acceleration (b ₂)	8.79E-06	6.73E-06	-1.37E-05
Neutral line orientation (b ₃)	9.85E-04	-6.72E-04	-1.04E-04
Flare importance factor (b ₄)	5.55E-08	-5.54E-08	-6.24E-08
Position (longitude) (b ₅)	2.48E-06	1.42E-05	1.70E-05

Position (latitude) (b ₆)	-5.86E-05	4.99E-05	1.41E-05
Magnetic classification RA (b ₇)	3.05E-04	-8.24E-05	7.97E-04
B (b ₈)	2.76E-05		-5.94E-05
Bz (b ₉)	-3.61E-04		1.08E-04
V _{tt} (b ₁₀)		-2.11E-05	-1.82E-06
v _{exp} (b ₁₁)		6.87E-07	4.30E-07

We also analysed the high speed stream from solar wind contribution to triggering the moderate geomagnetic storms from all four phases of the solar cycle 23. Comparing the HSS number that were produced by CH that triggered moderate geomagnetic storms during solar cycle 23, one can observe the large number in the descending phase (67) compared to the number of such events during the maximum phase (24), ascending (18) and, especially with minimum SC23 (only 10 events). The result concerning the time interval between minimum Dst and minimum Bz values we found, in this selection: one hour (36% events), two hours (21%), three hours (28%), and only 5 events (7%) with longer duration 4-6 hours and only two cases with two minima were registered at the same time.

The correlation analysis led to the results listed in Table 3.6.

Table 3.6. The determination coefficient (R^2) of the maximum HSS speed and of Bz compared to the Dst variation in various phases of SC23

Cycle 23 Phase	(V _{max} , Dst)	(V _{max} *Bz, Dst)	(Δ V _{max} , Dst)	(Δ V _{max} *Bz, Dst)
Minim	0.0071	0.7019	0.0073	0.0000
Ascending	0.0005	0.4235	0.0425	0.0000
Maxim	0.0010	0.7013	0.0135	0.0000
Descending	0.0625	0.2993	0.0245	0.0000

References

Besliu-Ionescu, D., Mierla, M., Maris Muntean, G., 2016, Analysis of the Energy Transferred from the Solar Wind into the Magnetosphere during the April 11, 2001 Geomagnetic Storm, *Sun and Geosphere*, 11, 101-108.

- Carrington, R., 1859, Singular Appearance in the Sun, *Monthly Notices of the Royal Astronomical Society*, 20, 13.
- Eselevich, V.G. și Fainshtein, V.G., 1991, The heliospheric current sheet (HCS) and high-speed solar wind - Interaction effects, *Planet. Space Sci.*, 39, 8, 1123-1131.
- Gupta, V., și Badruddin, H., 2010, High-Speed Solar Wind Streams during 1996 – 2007: Sources, Statistical Distribution, and Plasma/Field Properties, *Solar Phys.*, 264, 165-188.
- Hodgson, R., 1859, Curious Appearance in the Sun, *Monthly Notices of the Royal Astronomical Society*, 20, 15.
- Lindblad, B.A., și Lundstedt, H., 1981, A catalogue of high-speed plasma streams in the solar wind, *Solar Phys.*, 74, 197-206.
- Lindblad, B.A., și Lundstedt, H., 1983, A catalogue of high-speed plasma streams in the solar wind 1975–1978, *Solar Phys.*, 88, 377-382.
- Lindblad, B.A., și Lundstedt, H., 1989, A third catalogue of high-speed plasma streams in the solar wind. Data for 1978-1982, *Solar Phys.*, 120, 142-152.
- Mavromichalaki, H., Vassilaki, A., și Marmatsouri, A., 1988, A catalogue of high-speed solar-wind streams: further evidence of their relationship to Ap-index, *Solar Phys.*, 115, 345-365.
- Mariș, O. and Crosby, N., 2012, *Space environment effects on space- and ground-based technological systems*, in: *Advances in Solar and Solar-Terrestrial Physics*, Editors: G. Maris and C. Demetrescu, Research Signpost Publishers, Cap. 15, 293-328.
- Mariș, O. și Mariș, G., 2009, <http://www.spaceweather.eu/en/datacatalogue/>; http://www.spacescience.ro/new1/HSS_Catalogue.html
- Mariș, O. și Mariș, G., 2010, http://www.spacescience.ro/new1/GS_HSS_Catalogue.html
- Maris, G., Maris, O., 2001, Fast Solar Wind and Geomagnetic Variability during the Descendant Phase of the 11-yr Solar Cycle, *AIP Conf. Proc.* 1356, 177-183.
- Maris, G., Maris, O., 2012, High speed streams in the solar wind during the 23rd solar cycle, in: *Advances in Solar and Solar-Terrestrial Physics*, Editors: G. Maris și C. Demetrescu, Research Signpost Publishers, Cap. 7, 97-134.
- Maris, G., Maris, O., Oprea, C., Mierla, M., 2012, High-speed streams in the solar wind during the last solar minimum, *IAU Symposium*, 286, 229-233.
- Mavromichalaki, H. și Vassilaki, A., 1998, Fast plasma streams recorded near the Earth during 1985–1996, *Solar Phys.*, 183, 181-200.

- Mierla, M., Davila, J., Thompson, W., Inhester, B., Srivastava, N., Kramar, M., St Cyr, O.C., Stenborg, G., Howard, R.A., 2008, A Quick Method for Estimating the Propagation Direction of Coronal Mass Ejections using STEREO-COR1 Images, *Solar Phys.*, 252, 385–396.
- Mierla, M., Inhester, B., Marque, C., Rodriguez, L., Gissot, S., Zhukov, A., Berghmans, D., Davila, J., 2009, On 3D Reconstruction of Coronal Mass Ejections: I Method description and application to SECCHI-COR Data, *Solar Phys.*, 259, 123–141.
- Mierla, M., Inhester, B., Antunes, A., Boursier, Y., Byrne, J.P., Colaninno, R., Davila, J., deKoning, C.A., Gallagher, P.T., Gissot, S., et al., 2010, On the 3D reconstruction of coronal mass ejections using coronagraph data, *Ann. Geophys.*, 28, 203–211.
- Mierla, M., Inhester, B., Rodriguez, L., Gissot, S., Zhukov, A., and Srivastava, N., 2011, On 3D reconstruction of coronal mass ejections: II. Longitudinal and latitudinal width analysis of 31 August 2007 event, *J. Atm. Solar-Terr. Phys.*, 73, 1166-1172.
- Oprea, C., Mierla, M., și Maris, G., 2012, Earth-directed Coronal Mass Ejections and their Geoeffectiveness during the 2007 – 2010 Interval, IAU Symposium 286: Comparative Magnetic Minima: Characterizing quiet times in the Sun and stars, 3-7 October 2011, Mendoza, Argentina, Astronomical Union, *IAU Symposium*, 286, 242-245.
- Richardson I. și Cane, H., 2010, Near-Earth Interplanetary Coronal Mass Ejections During Solar Cycle 23 (1996--2009): Catalog and Summary of Properties, *Solar Phys.*, 189-197.
- Srivastava, N.și Venkatakrishnan, P., 2004, Solar and interplanetary sources of major geomagnetic storms during 1996-2002, *J. Geophys. Res.*, 109, A10103.
- Srivastava, N., 2005, A logistic regression model for predicting the occurrence of intense geomagnetic storms, *Annales Geophysicae*, 23, 2969–2974.
- St. Cyr, O. C., Burkepile, J. T., Hundhausen, A. J., and Lecinski, A. R., 1999, A comparison of ground-based and spacecraft observations of coronal mass ejections from 1980-1989, *Journal of Geophysical Research*, 104, 12493–12506.
- Zhang, J., Richardson, I. G., Webb, D.F., Gopalswamy, N., Huttunen, E., Kasper, J. C., Nitta, N. V., Poomvises, W., Thompson, B. J., Wu, C.-C., Yashiro, S., Zhukov, A. N., 2007, Solar and interplanetary sources of major geomagnetic storms (Dst 100 nT) during 1996–2005, *J. Geophys. Res.*, 112, A10102.

Chapter IV. Modeling the geomagnetically induced currents (GIC) by geomagnetic storms produced by solar eruptive phenomena

The interaction of the solar wind and of the heliospheric magnetic field with the magnetosphere and ionosphere results in variations of the geomagnetic field that induce hazardous electric currents in grounded technological systems (electric energy transport, hydrocarbon transport pipelines), the so-called geomagnetically induced currents (GIC). To evaluate the hazard affecting the European continent, we analysed the case of the surface geoelectric field induced by 16 intense geomagnetic storms occurred in the solar cycle 23 (1996-2008), characterized by a geomagnetic index $Dst < -150$ nT, based on recordings provided by the geomagnetic observatories of the European network. We explored in detail the evolution and sources of the disturbed field during the strongest geomagnetic storm of the solar cycle 23, namely the November 20-21, 2003 one, characterized by a Dst index of -422 nT, as well as the geographical distribution of the maximum surface geoelectric field induced by each of the 16 considered storms. A similar study has been performed for the storm of March 17, 2015, the strongest in the solar cycle 24, much studied in the literature though it was less intense ($Dst = -223$ nT) than the ones in solar cycle 23, because the estimation of terrestrial effects of the coronal mass ejection that caused it, based on the speed and direction of propagation of the CME when launched from the Sun, indicated insignificant possible values. In Fig. 4.1, the warning message issued by SIDC (Solar International Data Center), Belgium, is reproduced.

FAST WARNING 'PRESTO' MESSAGE from the SIDC (RWC-Belgium)

A partial halo coronal mass ejection (CME) was reported by CACTus and first seen in LASCO/C2 images at 02:00UT on 15-Mar-2015. This CME was related to a C9.1 flare from NOAA 2297 peaking at 02:13UT. The related CME had a plane of the sky speed of 712 km/s, and a width of 160 degrees. The bulk of the CME is directed away from Earth to the West, but a glancing blow can not be ruled out based on current imagery. The CME is estimated to arrive at Earth on 16 March at 18:00UT (+/- 12 hours).

Figure 4.1. Warning message issued by SIDC (Belgium)

4.1. Data and method

In the present study 1-minute values of geomagnetic elements X (northern component) and Y (eastern component) provided by 29 geomagnetic observatories of the INTERMAGNET network for a 6 days time interval that included the 16 analysed storms (Table 4.1) were used. Geomagnetic data have been processed by means of a code developed during the 2014 stage and improved in later stages of the project, in order to obtain the time derivative of the geomagnetic field and the surface electric field controlled by it. The electrical conductivity of the interior was estimated using the results of the European project EURISGIC (www.eurisgic.eu) and our project results presented in Chapter II. For the Romanian territory, the recordings from the Surlari geomagnetic observatory, a member of the INTERMAGNET network, for the major storm of November 20-21, 2003, as well as conductivity values determined in this project for the 26 stations of the Secular Variation National Network, presented in Chapter II, were used. The induced surface geoelectric field was calculated by the method of Viljanen and Pirjola (1989), shortly described in the following.

In general, the horizontal electric field (E_x , E_y) produced by the variable geomagnetic field (B_x , B_y) through the impedance $Z(\omega)$ of the Earth's interior, subject to the action of the plane wave that approximates the depth propagation of the geomagnetic disturbance, is given by:

$$E_x(\omega) = \frac{Z(\omega)}{\mu_0} B_y(\omega), E_y(\omega) = \frac{Z(\omega)}{\mu_0} B_x(\omega)$$

For a half-space Earth of conductivity σ , the surface electric field is described by

$$E_y(t) = -\frac{1}{\sqrt{\pi\mu_0\sigma}} \int_{-\infty}^t \frac{g_x(u)}{\sqrt{t-u}} du,$$

where g_x is the time derivative of the field B. The integral is transformed in a sum that allows calculating 1-minute values of the electric field E, by means of the above mentioned code. For denser networks two methods are currently in use (Viljanen et al., 2014) and (Matandirotya et al., 2014).

Table 4.1. The major geomagnetic storms of solar cycle 23

Year	Date	Dst (nT)	Year	Date	Dst (nT)
1998	May, 4	-205	2001	Apr, 11	-271
1998	Sep, 25	-207	2001	Nov, 5	-292
1999	Oct, 21	-237	2001	Nov, 24	-221
2000	Apr, 6	-287	2003	Oct, 29	-383
2000	Jul, 15	-301	2003	Nov, 20	-422
2000	Aug, 12	-235	2004	Nov, 7	-374
2000	Sep, 17	-201	2005	May, 15	-247
2001	March, 31	-387	2005	Aug, 24	-184

4.2. Results at the European continent scale

The largest storm of cycle 23, namely the November 20-21, 2003 one, with Dst = -422 nT, was produced by the interaction with the magnetosphere of an interplanetary coronal mass ejection (ICME), illustrated in Fig. 4.2 by means of solar wind parameters recorded at the Lagrangean Point 1, available on the site <http://omniweb.gsfc.nasa.gov/>. The evolution of the heliospheric magnetic field B, of its Bz component, and of the density, speed and dynamic pressure of the solar wind (N, V, and respectively Pw) is shown. The storm evolution is also shown, by means of the geomagnetic index Dst. The evolution of CME of the chain: solar flare – CME – ICME – geomagnetic storm is illustrated in Fig. 3.1, Chapter III.

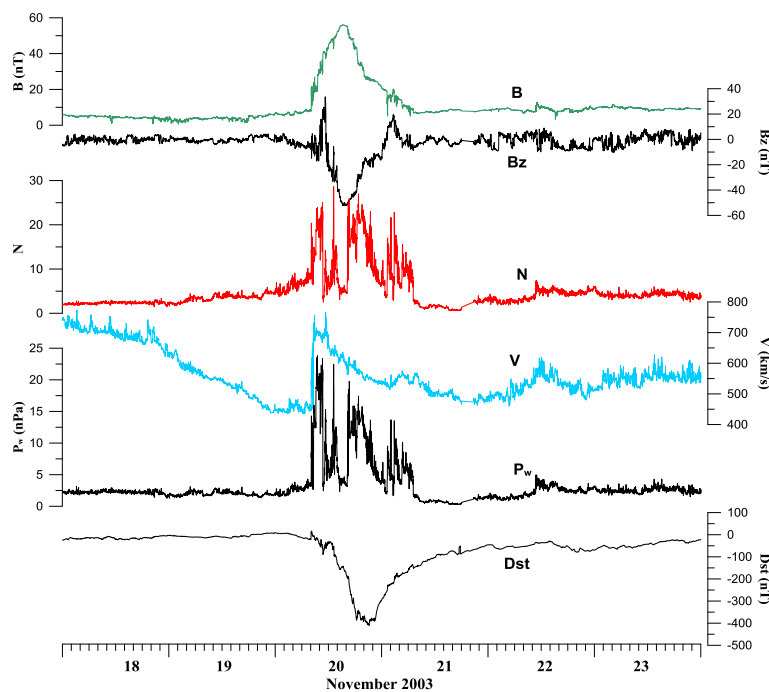


Figure 4.2. Evolution of solar wind parameters and of the Dst index for the November 20-21, 2003 geomagnetic storm

To estimate latitudinal differences that characterize the evolution of the geomagnetic field and of its time derivative, as well as of the surface geoelectric field induced by the geomagnetic storm, we show in Fig. 4.3 the results for a longitudinal chain of geomagnetic observatories along the 105°E geomagnetic meridian. The geomagnetic indices AL and Dst are also plotted, to illustrate maximum possible variations of the disturbing magnetic field. The AL index illustrates the disturbance produced by the ionospheric auroral electrojet, while the Dst index stands for the disturbance produced at the geomagnetic equator by the magnetospheric ring current.

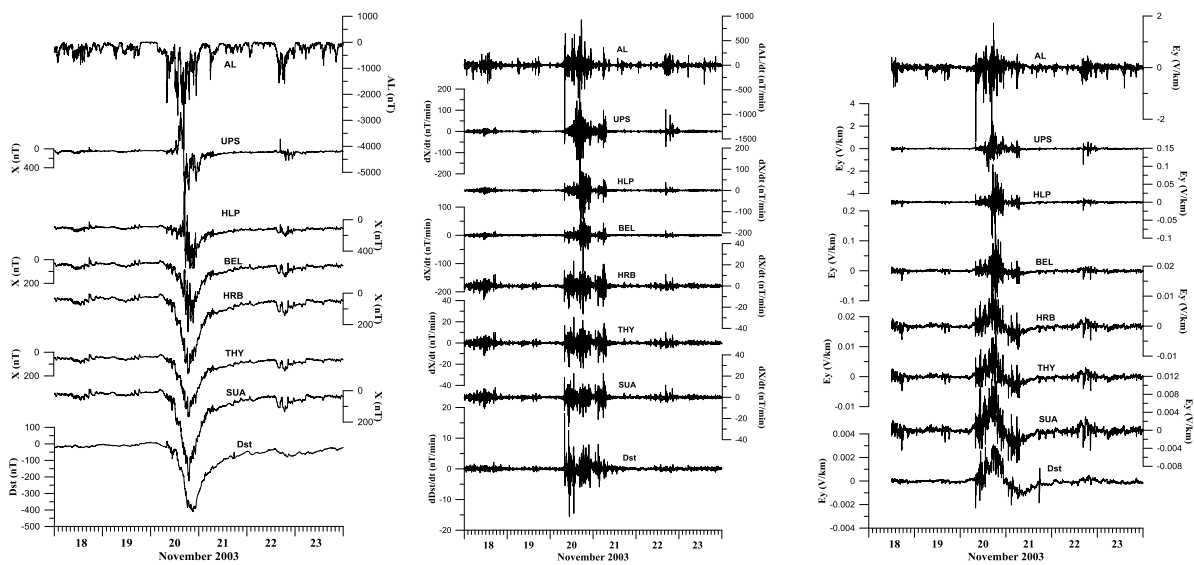


Figure 4.3. Geomagnetic disturbance (B_x) (left), its time derivative (middle), and surface geoelectric field (E_y) (right) for the November 20-21, 2003 storm, at geomagnetic observatories along the 105°E geomagnetic meridian

Some conclusions can be drawn from the figure, namely:

- The disturbance in B_x is 2-3 times larger at northern latitudes than at middle and southern ones;
- During the geomagnetic storm the effects of the auroral electrojet superimpose at all latitudes on the disturbance created by the magnetospheric ring current;
- The amplitude of the geoelectric field produced by geomagnetic variations is of the order of several hundredth V/km at SUA observatory (45°N) and of 1-2 V/km at the UPS observatory (60°N);
- The largest geoelectric component is E – W oriented.

The surface electric field was calculated for each European observatory considered, for various moments of the storm evolution in its initial and main phase (36 moments, at 30 minutes intervals). For each of the moments, maps of the electric field distribution were drawn. In Fig. 4.4 we give a few of them, as an example.

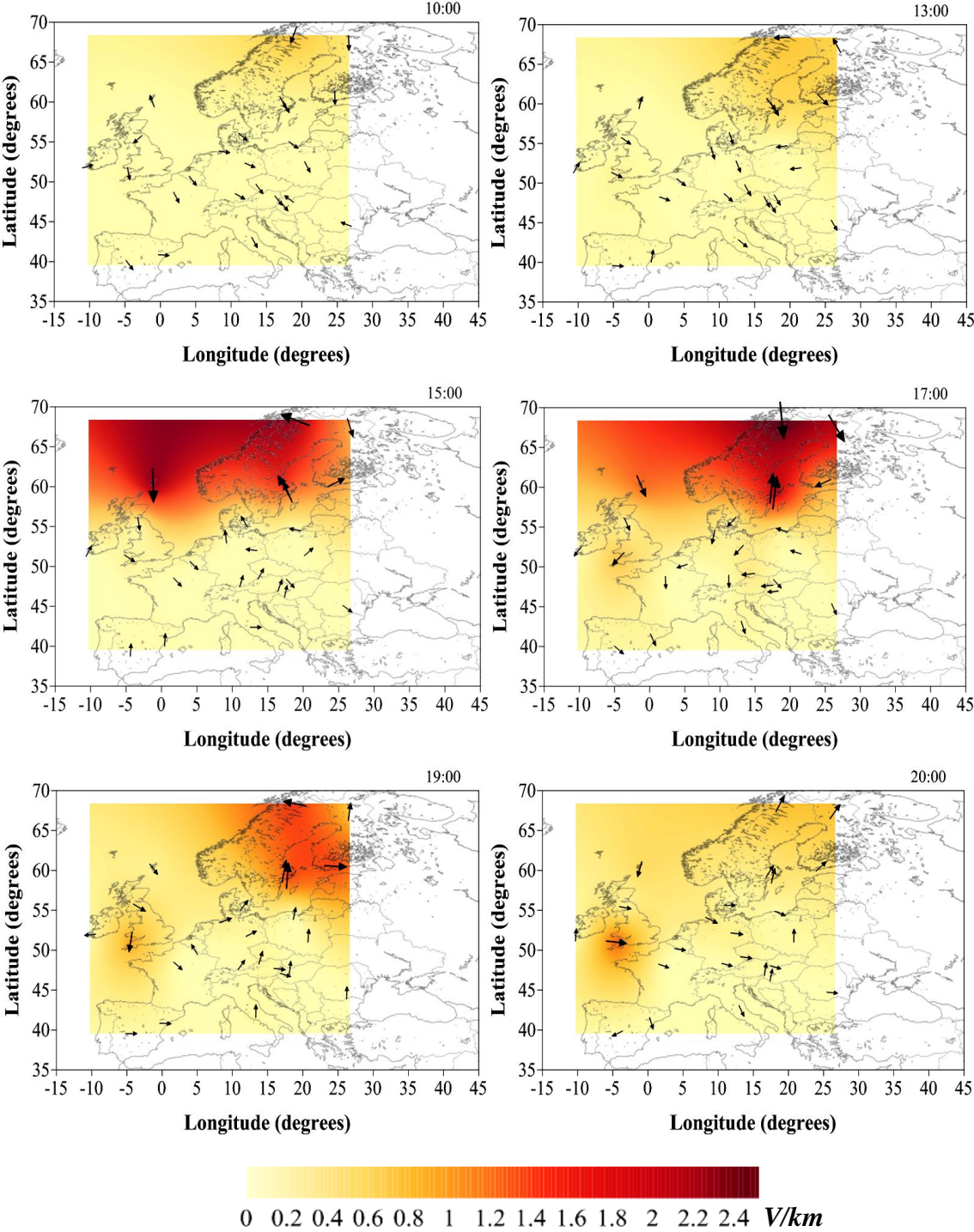


Figure 4.4. Examples of electric field maps during the initial and the main phase of the November 20-21, 2003 storm. Corresponding moments are marked. The field orientation is indicated by arrows, and the field magnitude corresponds to the color code or the arrow size

The maps of Fig. 4.4 show that (1) the largest disturbances occur in Scandinavia and, to a lesser extent in England and western France and (2) the direction of the field varies much during the storm and is not necessarily the same at all points at a given moment in the storm evolution.

As regards the source of the observed variations, our studies indicate both the magnetospheric ring current and the ionospheric auroral electrojet. Details have been presented in project stage reports.

In the end, as a next step in assessing the GIC type of hazard for the European territory, we calculated the maximum geoelectric field and its orientation at the observatories of the network, for each of the 16 geomagnetic storms considered in this project. The corresponding maps are shown in Fig. 4.5.

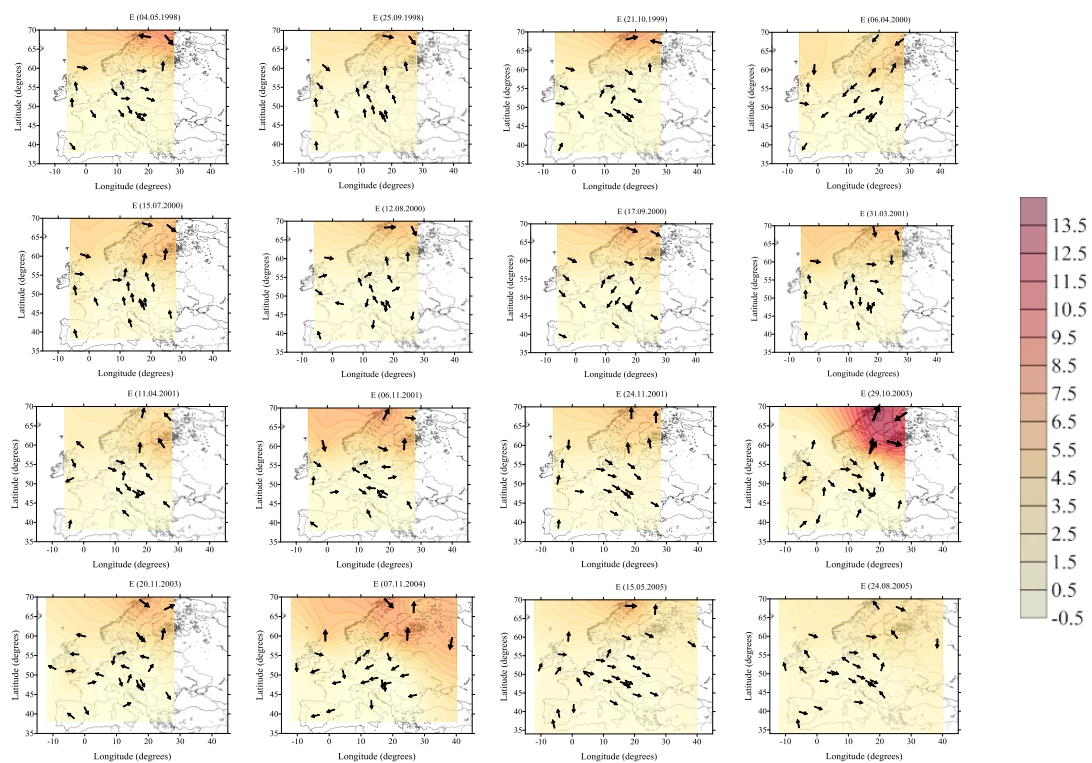


Figure 4.5. Maps of the maximum induced geoelectric field at the European observatories, for each of the 16 considered storms

The maximum value of E is not reached at the same moment at all observatories. Fig. 4.5 shows that the direction of the maximum induced electric field is not the same at all observatories, depending on the respective moment in the storm evolution.

4.3. Results for the Romanian territory

Being the most intense in the solar cycle 23 (1996-2008), the major geomagnetic storm of November 20-21, 2003 allows an assessment on the hazard for a time interval of 10-12 years represented by the surface electric field induced by such phenomena. To estimate the maximum surface electric field induced by the mentioned geomagnetic storm, the information on the distribution of the lithosphere electrical conductivity on the Romanian territory (Chapter 2), together with the recorded values during the storm at the Surlari geomagnetic observatory, were used. Evolution of the horizontal component at the Surlari geomagnetic observatory, in case of the the storm of November 20-21, 2003 is given in Fig. 4.6. The maximum intensity of the surface geoelectric field induced by the geomagnetic storm is given in Fig. 4.7. The map of this figure is equivalent to the geoelectric hazard distribution on the Romanian territory for a 12-year time interval, 1996-2008.

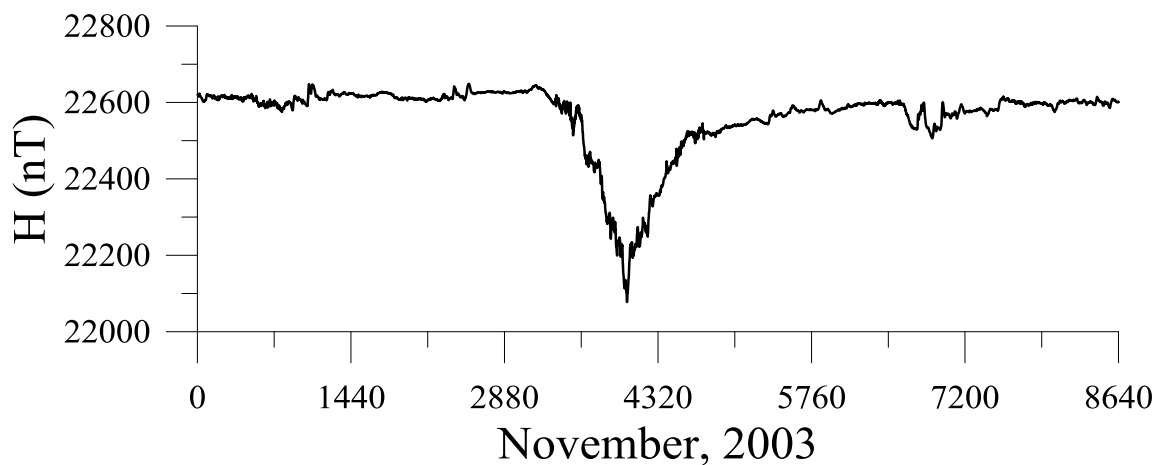


Figure 4.6. Evolution of the horizontal component at the Surlari geomagnetic observatory, the storm of November 20-21, 2003 included

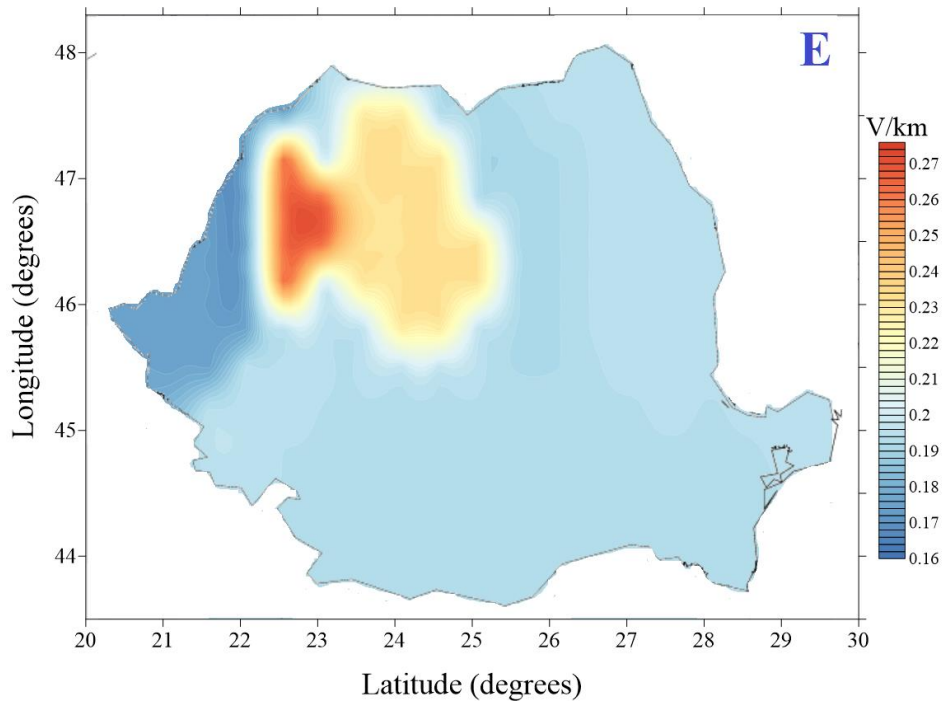


Figure 4.7. Maximum intensity of the surface geoelectric field induced by the geomagnetic storm of November 20-21, 2003 / Distribution of the geoelectric hazard for the solar cycle 23 (1996-2008)

Evaluation of the geophysical effects of major geomagnetic storms in the solar cycle 23 (1996-2008) is a first step of solving the problem of the hazard related to the occurrence of dangerous electric currents in electrical energy transport networks. Estimation of the actual currents that occur in concrete technological networks is the engineering part of the problem and asks for inclusion in the study real data regarding the network under evaluation. The part of the problem approached in this project will be detailed in a PhD study, begun however within the frame of this project.

References

Matandirotya, E., Cilliers, P. J., Van Zyl, R. R., 2015, Modelling geomagnetically induced currents in the South African power transmission network using the finite element method, *Space Weather*, doi: 10.1002/2014SW001135.

Viljanen, A. and Pirjola, R., 1989, Statistics on geomagnetically-induced currents in the Finnish 400 kV Power system based on recordings of geomagnetic variations, *J. Geomag. Geoelectr.*, 41, 411-420.

Viljanen, A., Pirjola, R., Pracser, E., Katkalov, J., Wik, M., 2014, Geomagnetically induced currents in Europe, *J. Space Weather Space Clim.*, 4, A09, doi: 10.1051/swsc/2014006.

Chapter V. On the geoeffectivity of solar activity before the space era

The so-called space era in space weather studies began in the decade 50-60' of the previous century, when space missions have been launched, destined to *in situ* measurements of parameters characterizing the solar wind and the interplanetary (heliospheric) magnetic field. The cause – effect relationship between the solar activity and the geomagnetic one has been known for a long time; as a matter of fact, the study of some geomagnetic phenomena, such as the magnetic storms and substorms, bays, pulsations, together with solar observations and studies, made the progress in solar physics and the development of the solar-terrestrial science possible. The space era has brought a large volume of *in situ* data on the corpuscular and radiative outputs of the Sun, as well as on the heliospheric magnetic field in which the magnetosphere is embedded, on one hand, and on processes that develop in the Sun and at its surface, on the other. Data from geomagnetic observatories are used to calculate various geomagnetic indices that stand as proxies to describe the evolution of current systems that develop in magnetosphere and ionosphere as a result of interaction of the solar wind with the geomagnetic (magnetosphere) field. Such indices are Dst, for variations caused in the geomagnetic equatorial zone by the magnetospheric ring current, or AE (with derived AU, AO, AL indices), for the geomagnetic field variations caused by the ionospheric auroral electrojets. To characterize the interplanetary electric field, of importance for estimating the energy transferred from the solar wind to magnetosphere, the PC index is used. To describe the geomagnetic activity at midlatitudes the *aa* and *Ap* indices are used (Fig. 5.1). While for the *aa* index the time series begins at 1868, the other indices have much shorter series (*Ap* – 1932; Dst, AE – 1957; PC - 1980). Research previous to the contract (Demetrescu and Dobrica, 2008; Demetrescu et al., 2010) showed that various geomagnetic indices correlate with each other, meaning that the current systems they describe vary in phase, indicating a common source, namely the solar dynamo. Svalgaard and Cliver (2005; 2007), Rouillard et al. (2007), Demetrescu et al. (2010) showed that geomagnetic indices IDV and *aa* can be used, due to their correlation to the heliospheric magnetic field *B*, and respectively to the product BV^2 , where *V* is the solar wind speed, as proxy for the temporal evolution of the two quantities (*V* and *B*) for the time period prior to space era.

In the present chapter we show results of attempts to characterize the **space climate** (variations of the geomagnetic, heliospheric, and solar activities at interannual, decadal, and centennial timescales).

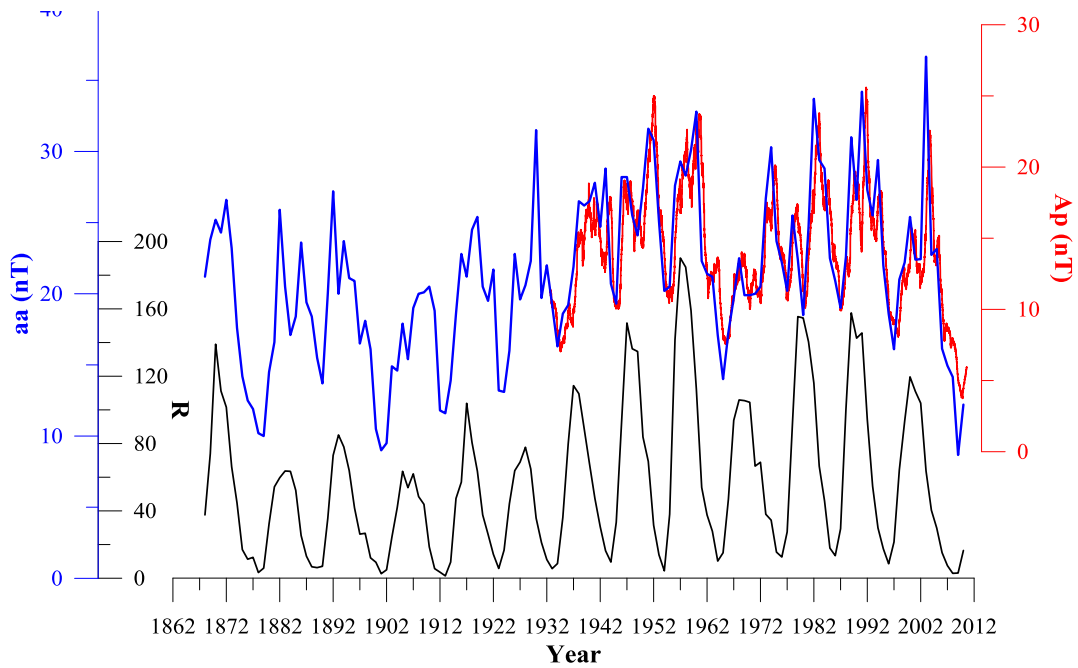


Figure 5.1. Evolution of geomagnetic activity (*aa* and *Ap* indices) as compared to solar activity (sunspot time series) for the last 150 years

In the following we present (1) an approach based on the correlation between the geomagnetic indices and parameters characterizing the solar wind, to reconstruct the evolution of the interplanetary merging electric field in the last 150 years, and (2) an approach on the variation of the geoeffectivity of solar activity in the last 400 years, based on the analysis of the *gufm1* (Jackson et al., 2000) model for the main (core) geomagnetic field.

5.1. Evolution of the interplanetary electric field in the last 150 years

In this section we present results of analyzing the effects the variations in the merging interplanetary electric field E_m (called geoeffective electric field) have on the magnetospheric and ionospheric current systems. Such effects could lead to dangerous disturbances of the geomagnetic and geoelectric fields (geomagnetic/geoelectric hazards). E_m forms as a result of the solar wind charged particles motion in the presence of the interplanetary (heliospheric) magnetic field. In the analysis the PC geomagnetic index was used as a measure of the merging electric field, in relation to other geomagnetic indices that describe the general disturbed state of magnetosphere and ionosphere (*aa* and *Ap*). The PC index has been recently defined (1980); it is built based on permanent recording of the geomagnetic field at the North polar cap station Thule of the Space Science Institute, Denmark, in such a way that following the statistical processing of the geomagnetic records and of solar wind and heliospheric magnetic field data, PC reflects the interplanetary geoeffective electric field E_m ,

$PC \sim Em = V_{SW} * B_T * (\sin(q/2))^2$, where $q = \arccos(B_z/B_T)$.

The main conclusion, that indices PC, Dst, AE aa, and Ap well correlate with each other at the interannual timescale and that the correlation is improving if the 11-year solar cycle effect is removed from data, allowed the reconstruction of the PC evolution back in time to 1868 (Fig. 5.2).

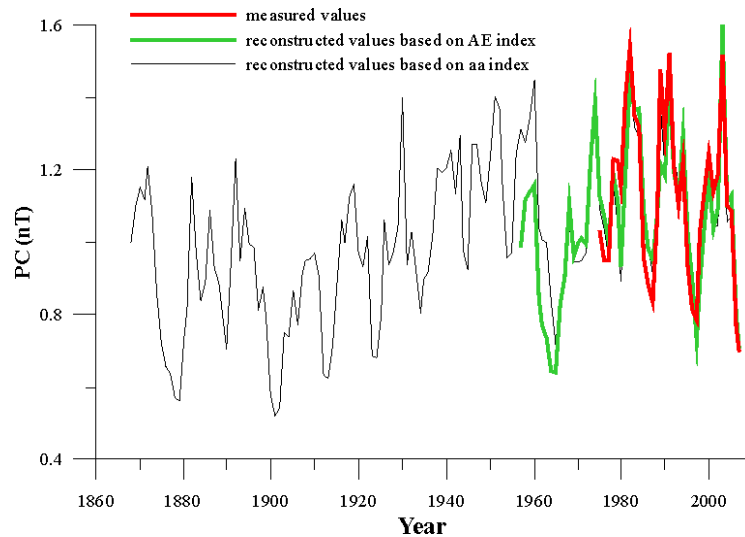


Figure 5.2. Reconstruction of the PC index, based on AE and *aa* indices

5.2. On the geoeffectivity of solar activity in the last 400 years

The research we shortly present in this section is based on two observations regarding some models for the main (core) geomagnetic field, namely: (1) the annual mean values of geomagnetic elements provided by geomagnetic observatories, that are the input in modeling, are contaminated by the incomplete averaging out of geomagnetic storm effects; (2) the contribution of external sources (mainly the magnetospheric ring current) to annual mean values is also found in the coefficients of the spherical harmonic model that represents the surface field distribution, if variations of external origin are not eliminated from the input data of the model.

We used the *gufm1* (Jackson et al., 2000) model, by which the evolution of the geomagnetic field for the time interval 1590 - 1990 is obtained. The model allows the construction of the time series for any given point on the Earth's surface. From such timeseries the constituent at the decadal timescale, considered by us as generated by external sources, mainly by the magnetospheric ring current, is extracted by filtering. In Fig. 5.3 we show such a time series, for the location of the Niemegek geomagnetic observatory, choice that

allows also a comparison with measured values. A first result is the presence of the geomagnetic activity during the well known solar activity minima (Maunder, 1645-1715, and Dalton, 1790-1830), that demonstrates the existence of solar cycles even in times of strongly decreased solar activity.

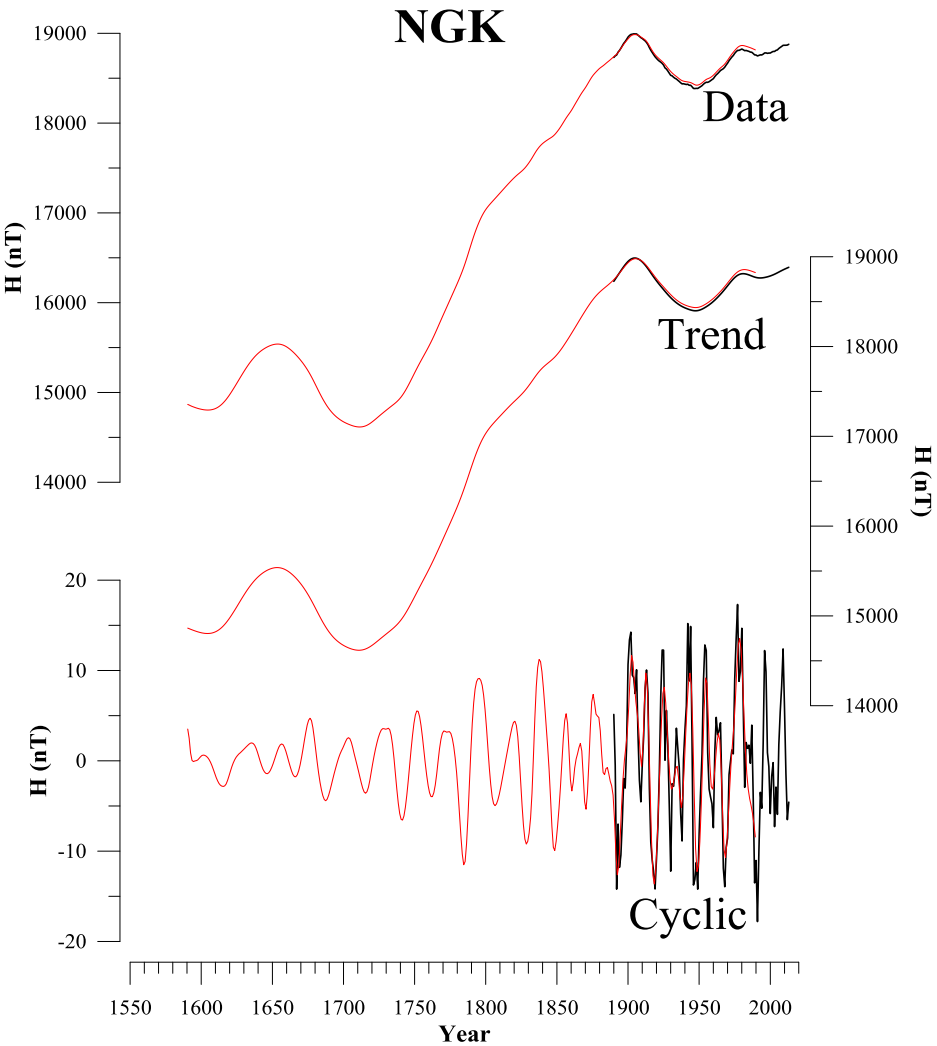


Figure 5.3. Variation at decadal timescale, related to the solar cycle modulated geomagnetic activity, for the location of the Niemegk geomagnetic observatory. Black – measured values; red – calculated values (*gufm1*). The Hodrick-Precott filtering was used

The preliminary result of this study opens a new perspective on research regarding the space climate and space weather, that will be continued and developed in future by the research team of the present project.

References

- Demetrescu, C. și Dobrica, V., 2008, Signature of Hale and Gleissberg solar cycles in the geomagnetic activity. *J. Geophys. Res.* 113, A02103, doi:10.1029/2007JA012570.
- Demetrescu, C., Dobrica, V., Mariș, G., 2010, On the long-term variability of the heliosphere–magnetosphere environment, *Advances in Space Research*, 46, 1299–1312.
- Jackson, A., Jonkers, A.R.T., Walker, M.R., 2000, Four centuries of geomagnetic secular variation from historical records. *Philos. Trans. R. Soc. London* 358, 957–990.
- Rouillard, A.P., Lockwood, M., Finch, I., 2007, Centennial changes in the solar wind speed and in the open solar flux. *J. Geophys. Res.* 112, A05103, doi:10.1029/2006JA012130.
- Svalgaard, L., Cliver, E.W., 2005, The IDV index: its derivation and use in inferring long-term variations of the interplanetary magnetic field strength, *J. Geophys. Res.*, A 110, doi:10.1029/2005JA011203.
- Svalgaard, L., Cliver, E.W., 2007, Interhourly variability index of geomagnetic activity and its use in deriving the long-term variation of solar wind speed, *J. Geophys. Res.* 112, A10111, 32 pp., doi:10.1029/2007JA012437.

Chapter VI. Results dissemination

In the time interval covered by the present contract (2011-2016), working stages have been performed, by the project director, Crişan Demetrescu, at the Department of Environmental Sciences, St. Mary University, Halifax, Canada, and by the PhD student Răzvan Greculeasa at Bonn University, Germany, on problems of time series analysis and testing methods for the significance level of two time series correlation.

During the project, two PhD theses have been finalized, one regarding the theoretical and modeling part of the geomagnetic field on the Earth's surface and its morphology at the core-mantle boundary, with implications in producing and characterizing the so-called geomagnetic jerks (Cristiana Ştefan, *High frequency evolutions in the secular variation of the geomagnetic field*), and the second, regarding characterization of the Earth's interior magnetic and electric properties, based on geomagnetic data recorded in the Secular Variation National Network stations and in the European network of geomagnetic observatories (Răzvan Greculeasa, *Contributions to the study of magnetic and electric properties of the Earth's interior based on geomagnetic measurements. Case studies – the Romanian territory, the European continent*)

During the project, the members of the research team actively participated to a number of international scientific conferences (European Union of Geosciences - EGU, Asia-Oceania Association of Geosciences - AOGS, International Association of Geomagnetism and Aeronomy - IAGA, International Union of Geodesy and Geophysics - IUGG), presenting 67 scientific papers (oral and poster), that can be consulted on the web page of the project and in the section RST-Indicatori.

As regards ISI papers, one has already been published and two others are under evaluation. A number of papers (11) were published in other data bases indexed journals. The list follows:

1. Dobrica, V., Demetrescu, C., Greculeasa, R., Isac, A., On the crustal bias of repeat stations in Romania, *Annals of Geophysics*, 55 (6), 1145 – 1154, doi: 10.4401/ag-5442, 2012.
2. Dobrica, V., Demetrescu, C., Manda, M., Geomagnetic field declination: from decadal to centennial scales, *Journal of Geophysical Research B*, 2014, under evaluation.

3. Stefan, C., Dobrica, V., Demetrescu, C., Magnetic flux patches at the core surface. Evolution in the last 400 years at sub-centennial time scale, *Geophysical Research Letters*, 2016, under evaluation.
4. Dobrica, V., Demetrescu, C., Maris, G., Solar wind dynamic pressure and magnetopause stand-off distance before the instrumental era, *Sun and Geosphere*, 7(1), 45-48, 2012.
5. Stefan, C., Dobrica, V., Demetrescu, C., On the evolution of geomagnetic activity in the last 300 years. Implications regarding solar wind dynamic pressure and magnetopause standoff distance, *Sun and Geosphere*, 8(1), 7 -10, 2013.
6. Greculeasa, R.A., Dobrica, V., Demetrescu, C., Sources of Geomagnetic Activity at Mid-Latitudes: Case Study – European Observatories, *Sun and Geosphere*, 8(1), 11-14, 2013.
7. Beşliu-Ionescu, D., Mariş Muntean, G., Lăcătuş, D.A., Paraschiv, A.R., Mierla, M., Detailed Analysis of an Geoeffective Icme Triggered by the March 15, 2013 CME, *Romanian Geophysical Journal*, 56-57, 41-47, 2012-2013.
8. Stefan, C., Application of the Radon transform to the study of traveling speeds of core geomagnetic field features. Case study – The ~80-year variation, *Romanian Geophysical Journal*, 56-57, 11-15, 2012-2013.
9. Besliu-Ionescu, D., Mierla, M., Maris Muntean, G., Magnetic crochet associated to the seismically active flare of March 29, 2014, *Romanian Geophysical Journal*, 2015, accepted.
10. Greculeasa, R., Dobrica, V., Isac, A., The evolution of the geomagnetic field on the Romanian territory. Measurements in the secular variation national network between 2010 and 2014, *Romanian Geophysical Journal*, 2015, accepted.
11. Stefan, C., Dobrica, V., Demetrescu, C., Residual 11-year signal in coefficients of main field models, *Romanian Geophysical Journal*, 2015, accepted.
12. Besliu-Ionescu, D., Mierla, M., Maris Muntean, G., Analysis of the Energy Transferred from the Solar Wind into the Magnetosphere during the April 11, 2001 Geomagnetic Storm, *Sun and Geosphere*, 11(2), 97-104, 2016.
13. Dobrica, V., Demetrescu, C., Stefan, C., Greculeasa, R.A., Geomagnetically Induced Currents, a space weather hazard. Case study – Europe under intense geomagnetic storms of the solar cycle 23, *Sun and Geosphere*, 11(2), 111-117, 2016.

14. Besliu-Ionescu, D., Donea, A., Cally, P., Current State of the Seismic Emission Associated to Solar Flares, Sun and Geosphere, 2016, accepted.

The web page of the project, that contains information referring to the project description, to objectives and research stages, to the scientific team, as well as to results of the research, can be found at the address: <http://www.geodin.ro/IDEI2011/engl/index.html>.

Conclusions

In conditions in which problems related to space weather – the way in which phenomena and processes in the Sun and its atmosphere result in changes in heliosphere and in particular in the vicinity of Earth and at its surface – changes with important consequences for the human activity in space, for the space technology, and for the technological structures on the Earth's surface (electric networks, pipe networks, railways), strongly and strongly rise questions of hazards related to them, the present contract aimed at a better understanding the effects of space weather on the electrical conductive structures of the Earth's interior, with applications to improve the knowledge of the internal structure at the geographical scale of the Romanian territory and the European continent, on one hand, and to assess the geophysical hazard at midlatitudes corresponding to space weather processes, on the other. The main objectives of the contract were:

1. Determining the magnetic and electric structure of Earth's crust and mantle at the Romanian territory and European continent scales;
2. Analysis of solar eruptive processes and of the solar wind, responsible for the risk geomagnetic activity (geomagnetic storms and substorms) in the time interval 1964-2014;
3. Modeling of the surface geoelectric field;
4. Evaluation of the geophysical hazard associated to variations of the surface geoelectric field.

The main results of the research within the frame of the contract could be summarized as follows:

- Two methods to determine the electric properties of the Earth's interior, at the scales of the Romanian territory and of the European continent, were used, namely (1) the classical one, of magnetotelluric soundings, and (2) the magnetic induction model, developed by the research team prior to the present contract. The results allowed both the estimation of the geoelectric hazard produced by the space weather, for the two studied territories, for the solar cycle 23 (1996-2008), and evaluation of merits and demerits of the two employed methods;
- To update the data base and monitor the evolution of the geomagnetic field on the Romanian territory, as well as to update the magnetotelluric archive, geomagnetic and magnetotelluric measurements have been performed in each year of the contract. The geomagnetic values were used to infer the geographical distribution, the secular variation of

the geomagnetic field, and not in the least the magnetic and electric structure of the Earth's interior on the Romanian territory;

- Comparing the results of applying the two methods showed that the scale of the obtained information differs, in the sense that the magnetotelluric method solves problems at geographical scales represented by lithospheric blocks with dimensions of hundreds of kilometers, while the magnetic induction method gives information localized to positions of observatories and stations at which geomagnetic recordings are taken. In addition, the magnetotelluric method was limited in case of Europe to a depth of 80 km, while the investigated depth in the magnetic induction method regards the entire lithosphere;

- As regards the density of the information obtained, the magnetotelluric method could benefit from the densifying of the measurements network, while construction and maintaining of new geomagnetic is problematic, mainly from financial reasons. From the same reason, we do not envisage detailing the European scale magnetotelluric model, that should be done by each European country. The Romanian annual repeat station network needs the usual financing of IDEI-type projects.

- The study of the cause-effect link between solar eruptive processes and solar wind parameters, on one hand, and the geomagnetic storms/substorms, on the other, led to a synthesis for the solar cycle 23 (1996-2008) and, respectively, for the last four solar cycles, 20-23 (1964-2008);

- Data recorded by European geomagnetic observatories, members of the INTERMAGNET network that includes the Surlari observatory, have been used to characterize the geoelectric hazard induced by 16 major geomagnetic storms in solar cycle 23, and in the detailed study for the case of the largest storm in the cycle (20-21.11.2003), both at continental and Romanian territory scales;

- A study has been started on the space climate, a concept that treats the evolution of space weather at decadal, multidecadal, and centennial time scales, with results for the last 150 and the last 400 years, a start that could be developed in future research contracts;

- Not in the least, during the project 2 PhD theses have been finalized, 3 papers were published or are under evaluation in ISI indexed journals and 11 papers in journals indexed in other data bases. Also 67 papers were presented at important international scientific conferences.